

Hubble Tension and Cosmological Imprints of $U(1)_X$ Gauge Symmetry: $U(1)_{B_3-3L_i}$ as a case study

Dilip Kumar Ghosh,^{1,*} Purusottam Ghosh,^{1,†} Sk Jeesun,^{1,‡} and Rahul Srivastava^{2,§}

¹ *School of Physical Sciences, Indian Association for Cultivation of Science,
2A & 2B Raja S C Mullick Road, Kolkata 700032, India*

² *Department of Physics, Indian Institute of Science Education and Research - Bhopal
Bhopal Bypass Road, Bhauri, Bhopal, India*

Abstract

The current upper limit on N_{eff} at the time of CMB by Planck 2018 can place stringent constraints in the parameter space of BSM paradigms where their additional interactions may affect neutrino decoupling. Motivated by this fact in this paper we explore the consequences of light gauge boson (Z') emerging from local $U(1)_X$ symmetry in N_{eff} at the time of CMB. First, we analyze the generic $U(1)_X$ models with arbitrary charge assignments for the SM fermions and show that, in the context of N_{eff} the generic $U(1)_X$ gauged models can be broadly classified into two categories, depending on the charge assignments of first generation leptons. We then perform a detailed analysis with two specific $U(1)_X$ models: $U(1)_{B_3-3L_e}$ and $U(1)_{B_3-3L_\mu}$ and explore the contribution in N_{eff} due to the presence of Z' realized in those models. For comparison, we also showcase the constraints from low energy experiments like: Borexino, Xenon 1T, neutrino trident, etc. We show that in a specific parameter space, particularly in the low mass region of Z' , the bound from N_{eff} (Planck 2018) is more stringent than the experimental constraints. Additionally, a part of the regions of the same parameter space may also relax the H_0 tension.

*Electronic address: dilipghoshjal@gmail.com

†Electronic address: pghoshiitg@gmail.com

‡Electronic address: skjeesun48@gmail.com

§Electronic address: rahul@iiserb.ac.in

1. INTRODUCTION

The cosmological parameter N_{eff} , associated with the number of relativistic degrees of freedom, is crucial in describing the dynamics of the thermal history of the early universe. At very high temperature of the universe, the photon and electron bath were coupled, whereas at low temperature the interaction rate drops below the Hubble expansion rate and the two baths decouple [1]. N_{eff} is parameterised in terms of the ratio of energy densities of photon and neutrino bath. Within the Standard Model (SM) particle contents, the two aforementioned baths were coupled through weak interactions at high temperature and as temperature drops ($T \sim 2$ MeV) they decouple. Assuming such scenario the predicted value of $N_{\text{eff}}^{\text{SM}}$ turns out to be 3.046 [2, 3]. This value of N_{eff} deviates from the number of neutrinos (3) in the SM particle content is due to various non-trivial effects like non-instantaneous neutrino decoupling, finite temperature QED corrections and flavour oscillations of neutrinos [2, 3]. However, in observational cosmology also, measurements of the cosmic microwave background (CMB), baryon acoustic oscillations (BAO), and other cosmological probes provide constraints on N_{eff} . The current Planck 2018 data has precise measurement of N_{eff} at the time of CMB with 95% confidence level, $N_{\text{eff}} = 2.99_{-0.33}^{+0.34}$ [4]. Thus the current upper limit from Planck 2018 data shows that there can be additional contribution (apart from SM predicted value) to N_{eff} , indicating the scope for new physics.

It is evident that N_{eff} will change in the presence of any beyond standard model (BSM) particles with sufficient interactions with either of the photon or neutrino bath at temperatures relevant for neutrino decoupling [5–8] or in presence of any extra radiation [9–12]. Thus the upper limit on N_{eff} from CMB can be used to constrain such BSM paradigms dealing with any extra energy injection. Several studies have been performed to explore the imprints of BSM models in N_{eff} like models with early dark energy [10, 13], relativistic decaying dark matter [14] and non-standard neutrino interactions (NSI) [5, 6, 15–18]. From the perspective of neutrino physics, the last one is very interesting since the non-standard interactions of light neutrinos may alter the late-time dynamics between photon and neutrino baths, contributing to N_{eff} and the same NSI interactions can be probed from ground based neutrino experiments as well [19, 20].

On the other hand, the anomaly-free $U(1)_X$ gauge extended BSM models are well-motivated from several aspects like non zero neutrino masses [21], flavor anomalies [22] etc. The anomaly condition allows the introduction of right-handed neutrinos in the theory and thus it can also explain non-zero neutrino masses via the Type-I seesaw mechanism [21]. These scenarios naturally involve a gauge boson (Z') that originates from the $U(1)_X$ abelian gauge symmetry and has neutral current interactions with neutrinos and electrons which may have some nontrivial role in neutrino decoupling and hence in deciding N_{eff} [6, 7, 15, 23]. The detectability of gauge boson throughout the mass scale ($M_{Z'}$) also motivates such scenarios. For TeV-scale Z' , constraints arise from collider experiments [24–27], whereas in the sub-GeV mass region, low energy scattering experiments (neutrino electron scattering

[28], neutrino-nucleus scattering [29] etc.) are relevant to constrain the parameter space. However, both types of direct searches become less sensitive in the mass $M_{Z'} \lesssim \mathcal{O}(\text{MeV})$ and lower coupling ($g_X \lesssim 10^{-5}$) region. In that case, the CMB observation on N_{eff} plays a crucial role and can impose severe constraints on the $M_{Z'} - g_X$ plane, which stands as the primary focus of our study.

In cosmology, there exists some discrepancy between the values of expansion rate H_0 obtained from CMB and local measurement [4, 30–33]. Using direct observations of celestial body distances and velocities, the SHOES collaboration calculated $H_0 = 73.04 \pm 1.04 \text{ Km s}^{-1} \text{ Mpc}^{-1}$ [33]. However, the CMB measurements like Planck 2015 TT data predict $H_0 = 68.0_{-3.0}^{+2.6} \text{ Km s}^{-1} \text{ Mpc}^{-1}$ at 1σ [34] and from recent Planck 2018 collaboration it turns out to be $H_0 = 67.36 \pm 0.54 \text{ Km s}^{-1} \text{ Mpc}^{-1}$ [4], where both the collaboration analyzes the CMB data under the assumption of ΛCDM cosmology. So there is a disagreement between the local and CMB measurements roughly at the level of $4\sigma - 6\sigma$ [30]. Although such discrepancy may arise from systematic error in measurements [35, 36], it also provides a hint for BSM scenarios affecting the dynamics of the early universe. One possible way out to relax this so called “ H_0 tension” involves increasing N_{eff} in the approximate range $\sim 3.2 - 3.5$ [6, 37, 38]¹. As discussed earlier $U(1)_X$ local gauge extension leads to new gauge boson and new interaction with SM leptons which might affect neutrino decoupling and hence contribute to N_{eff} . Thus $U(1)_X$ gauge extension can be one possible resolution to the H_0 tension also. Two kinds of $U(1)_X$ scenarios have been considered so far in the literature to address the Hubble tension problem and/or the excess in N_{eff} at CMB: $U(1)_{\mu-\tau}$ [6] and $U(1)_{B-L}$ [7]. In both these two cases, the corresponding gauge boson mass lies below 100 MeV, which attracts severe constraints from scattering experiments [19, 20], energy loss in supernovae, etc [40]. Note that in the second scenario, $U(1)_{\mu-\tau}$, the light gauge boson couples to the μ and τ leptons but does not to the electron and quarks at the tree level. As a result, it is subject to less existing constraints than $U(1)_{B-L}$.

In this work, we begin with a generic $U(1)_X$ extension and explore the aforementioned cosmological phenomena more comprehensively. For simplicity, we assume the light gauge boson was in a thermal bath, and the right-handed neutrinos are heavy enough ($> \mathcal{O}(10^2)$ MeV) that they hardly play any role in neutrino decoupling. We study the dynamics of neutrino decoupling in the presence of the light gauge boson (Z') in a generic $U(1)_X$ scenario with arbitrary $U(1)_X$ charge assigned to SM fermions. We evaluate N_{eff} by solving a set of coupled Boltzmann equations that describe the evolution of light particles i.e. electron, SM neutrino, and light gauge boson ($M_{Z'} \lesssim \mathcal{O}(10)$ MeV). Thus we identify the region of parameter space that is consistent with Planck 2018 observations. We also illustrate the parameter space in which Hubble tension can be relaxed where the value of N_{eff} falls within the range of 3.2 to 3.5 [37]. Our analysis show that the depending on the $U(1)_X$

¹ However, it is essential to acknowledge that increasing N_{eff} also provokes the tension related to the other parameter of ΛCDM model, σ_8 [4, 39].

charge assignment of the first generation lepton, the generic $U(1)_X$ gauged models can be classified in context of N_{eff} . We incorporate these cosmological observations into specific gauged $U(1)_X$ models, $U(1)_{B_3-3L_i}$ ($i = e, \mu, \tau$). In comparison to others, these extensions encounter fewer constraints, as they are exclusively linked only to the third generation of quarks and one generation of leptons. Our results show that the upper limit on N_{eff} from Planck 2018 [4] can put stringent bounds on the parameter space of light Z' in the mass region $\lesssim 100$ MeV where the other experimental bounds are comparatively relaxed.

The paper is organized as follows. In sec.2, we begin with a brief model-independent discussion on the generic $U(1)_X$ model. Sec.3 is dedicated to a comprehensive analysis and discussion of the dynamics governing neutrino decoupling in terms of the cosmological parameter N_{eff} in the presence of the light Z' originated from the generic $U(1)_X$. Subsequently, in sec.4, we present the numerical results in terms of N_{eff} for this generic $U(1)_X$ model. In sec.5, we discuss the analysis presented earlier, which applies to the specific $U(1)_X$ model, $U(1)_{B_3-3L_i}$ ($i = e, \mu, \tau$). We present a brief discussion on H_0 tension in sec.6. Finally, in sec.7, we summarise and conclude with the outcomes of our analysis. In Appendices A to C, we provide various technical details for the calculation of N_{eff} .

2. MODEL INDEPENDENT DISCUSSION: EFFECTIVE Z' MODELS

In this section, we look at effective light Z' models. We take a model-independent but minimalist approach and only assume that the Z' originates from the breaking of a new local $U(1)_X$ abelian gauge symmetry under which the SM particles are charged as shown in Table I. The anomaly cancellation conditions for a typical $U(1)_X$ local gauge symmetry requires the presence of additional chiral fermions beyond the SM fermions². To keep the minimal scenario we assume that the only BSM fermions needed for anomaly cancellation are the (three) right handed neutrinos ν_R which are taken to be charged under the $U(1)_X$ symmetry. With the addition of ν_R , several different type of gauged $U(1)_X$ models including the popular $U(1)_X$ models such as the $U(1)_{B-L}$ or $U(1)_{\mu-\tau}$ can be constructed. We will discuss some of the models in the next Section 5.

For this purpose within this section, we will not specify the nature of $U(1)_X$ symmetry nor the charges of SM particles and ν_R under it and will treat them as free parameters and proceed with a generic discussion. We will also not go into details of anomaly cancellation constraints. All these things will be clarified in the following sections during our discussions on some well motivated $U(1)_X$ models. In Table I, in addition to ν_R (typically required

² Note that for one generation of SM fermions, the only $U(1)$ symmetry which is anomaly free is the SM hypercharge $U(1)_Y$ symmetry. For the full three generations of SM fermions, it is possible to have additional $U(1)_X$ symmetries which can be made anomaly free without adding any new chiral fermions such as $U(1)_{q_i-q_j}$; $i, j = 1, 2, 3$ with q_i, q_j denoting charges of a given generation of SM quarks but such symmetries have other phenomenological problems and are not of interest to the current study.

Fields	$SU(3)_c \times SU(2)_L \times U(1)_Y$	$U(1)_X$
Q_i	$(3, 2, \frac{1}{3})$	\mathbb{X}_{Q_i}
u_i	$(3, 1, \frac{4}{3})$	\mathbb{X}_{u_i}
d_i	$(3, 1, -\frac{2}{3})$	\mathbb{X}_{d_i}
L_i	$(1, 2, -1)$	\mathbb{X}_{L_i}
ℓ_i	$(1, 1, -2)$	\mathbb{X}_{ℓ_i}
ν_{R_i}	$(1, 1, 0)$	\mathbb{X}_{ν_i}
Φ	$(1, 2, 1)$	\mathbb{X}_Φ
σ	$(1, 1, 0)$	\mathbb{X}_σ

TABLE I: Particle content and $U(1)_X$ gauge charge assignments of Standard Model and new particles. In this section, we will take $\mathbb{X}_\Phi = 0$ as we are interested in a light Z' gauge boson.

for anomaly cancellation) we also add an SM singlet scalar σ carrying $U(1)_X$ charge whose vacuum expectation value (VEV) will break the $U(1)_X$ symmetry. Note that apart from the minimal particle content of Table I, most of the $U(1)_X$ models available in literature may also contain additional BSM particles³. These additional particles are model dependent and we refrain from adding them to proceed with a minimal setup.

Now some general model independent simplifications and conclusions can be immediately drawn for the charges of the particles under $U(1)_X$ symmetry listed in the aforementioned Table I.

1. **Light Z' :** In the upcoming sections, we delve into an effective resolution of the well-known Hubble parameter tension [37] by increasing N_{eff} considering a light Z' with mass $M_{Z'} \sim \mathcal{O}(\text{MeV})$ mass range[6]. To avoid any fine-tuning in keeping the $M_{Z'}$ very light compared to the SM Z gauge boson mass i.e. $M_{Z'}^2 \ll M_Z^2$, we consider the corresponding $U(1)_X$ charge of the SM Higgs doublet $\mathbb{X}_\Phi = 0$, so that $M_{Z'}^2$ does not receive any contribution from the SM vev.
2. **Mass generation for quarks and charged leptons:** For the choice of $\mathbb{X}_\Phi = 0$, to generate the SM quark and charged lepton masses, we must take $\mathbb{X}_{Q_i} = \mathbb{X}_{u_i} = \mathbb{X}_{d_i}$ and $\mathbb{X}_{L_i} = \mathbb{X}_{\ell_i}$ such that the standard Yukawa term $y_{ij}^u \bar{Q}_i \tilde{\Phi} u_j$ involving only SM fields can be written in the canonical form as shown in eq.(1). It is important to note that although within each generation, the $U(1)_X$ charges of quark doublet should be the same as that of the up and down quark singlets, the charges may differ when comparing across different generations i.e. $\mathbb{X}_{Q_1} \neq \mathbb{X}_{Q_2} \neq \mathbb{X}_{Q_3}$. The same applies to charged leptons. In fact, in later sections, we will indeed consider flavour dependent $U(1)_X$ symmetries. To simplify our notation throughout the remaining part of this paper we will denote $\mathbb{X}_{L_i} = \mathbb{X}_{\ell_i} = X_i$.

³ Such new particles are typically much heavier than MeV scale and will not change our analysis [22].

3. **Quark mixing:** As a follow up point note that if the charges of all three generations of quarks are unequal i.e. if we take $\mathbb{X}_{Q_1} \neq \mathbb{X}_{Q_2} \neq \mathbb{X}_{Q_3}$ then the Yukawa matrices Y^u and Y^d and hence the resulting mass matrices will only have diagonal entries and we will not be able to generate CKM mixing. Thus, the charges of some (but not all) generations should match with each other in order to allow the generation of quark mixing. The same is true for charged lepton mass matrices. Again we will elaborate it further with specific examples in the coming sections.
4. **BSM fermions:** The $U(1)_X$ charge of right handed neutrinos is typically fixed by anomaly cancellation conditions as we will discuss in a later section with specific examples. As mentioned earlier, for the sake of simplicity, we will not consider $U(1)_X$ symmetries involving chiral fermions beyond the fermion content of Table I.

Based on the aforementioned assumptions one can write the Yukawa and scalar potential for the general $U(1)_X$ model as:

$$\mathcal{L}_{Yuk} = y_{ij}^u \bar{Q}_i \tilde{\Phi} u_j + y_{ij}^d \bar{Q}_i \Phi d_j + y_{ij}^e \bar{L}_i \Phi \ell_j + \mathcal{L}_\nu + h.c. \quad (1)$$

and

$$V(\Phi, \sigma) = \mu_\Phi^2 \Phi^\dagger \Phi + \mu_\sigma^2 \sigma^\dagger \sigma + \lambda_\Phi \Phi^\dagger \Phi \Phi^\dagger \Phi + \lambda_\sigma \sigma^\dagger \sigma \sigma^\dagger \sigma + \lambda_{\Phi\sigma} \Phi^\dagger \Phi \sigma^\dagger \sigma \quad . \quad (2)$$

It is worth highlighting a couple of salient features of the Yukawa terms and the scalar potential of this scenario.

1. In eq.(1), \mathcal{L}_ν refers to the terms needed for light active neutrino mass generation. These terms depend on the details of the $U(1)_X$ symmetry, the charges of leptons under it as well as the nature of neutrinos (Dirac or Majorana) and the mechanism involved for mass generation. Furthermore, this typically requires the presence of additional scalars or fermions or both, beyond the particle content listed in Tab. I. Note that even in the massless limit and absence of any other interactions, the ν_R is still interacting with the rest of the particles through its $U(1)_X$ gauge interactions and depending on the charges and strength of the $U(1)_X$ gauge coupling (g_X), they can be in thermal equilibrium with the rest of the plasma at a given epoch in the evolution phase of the early universe.
2. Since we want a very light Z' , therefore the vev of σ field $\langle \sigma \rangle = v_\sigma$ which is responsible for Z' mass generation should be small. Furthermore, after SSB, if we want the real physical scalar σ_R to be light as well, we should have $\lambda_{\Phi\sigma} \ll 1$. The condition $\lambda_{\Phi\sigma} \ll 1$ will also imply that the 125 GeV scalar (h) is primarily composed of the real part of Φ^0 (neutral component of Φ) and hence the LHC constraints on it can be trivially satisfied.

With these general assumptions, one can examine the potential range of a Z' parameter that may account for the observed excess of N_{eff} in the Planck 2018 data, leaving the charge of the leptons and the gauge coupling as free parameters.

3. ν_L DECOUPLING IN PRESENCE OF LIGHT Z' AND N_{eff}

It is a well known fact that one of the most precisely measured quantities from cosmology is the effective neutrino degrees of freedom (N_{eff}), which may get altered by the presence of light BSM particles. This change in N_{eff} from the SM value can in principle provide one of the solutions to relax the Hubble tension [37]. In this work, we focus on a scenario with light Z' interacting with SM neutrinos (ν_i , ($i \equiv e, \mu, \tau$)) that may lead to change in N_{eff} . After having a brief description of generic features of light Z' models emerging from $U(1)_X$ symmetries in the previous section, we now move to the most crucial part of our paper which is the cosmological implications of those scenarios. Before delving into the analysis of N_{eff} in the presence of such light Z' , we would like to mention some key aspects of N_{eff} within the SM framework.

In a standard cosmological scenario at temperature $T \sim 20 \text{ MeV}$ ⁴, only e^\pm, ν_i are particles coupled to thermal (photon) bath as the energy densities of other heavier SM particles are already Boltzmann suppressed. As the universe cools, once the weak interactions involving e^\pm and ν_i drop below the Hubble expansion rate $H(T)$, neutrinos decouple from the photon bath. Considering only the SM weak interactions, the neutrino decoupling⁵ temperature turns out to be 2 MeV [1, 41]. After that, there exist two separate baths of photon ($+e$) and ν_i , each with different temperatures; T_γ and T_ν respectively. Approximately, at a temperature below $T_\gamma \lesssim 0.5 \text{ MeV}$, e^\pm annihilate, and the entropy is transferred entirely to photon bath leading to an increment in T_γ compared to neutrino bath. This difference in temperature is parameterised in terms of N_{eff} which is given by[1],

$$N_{\text{eff}} = \frac{8}{7} \left(\frac{11}{4} \right)^{4/3} \left(\frac{\rho_{\nu_L}(T_\nu)}{\rho_\gamma(T_\gamma)} \right) = 3 \times \frac{8}{7} \left(\frac{11}{4} \right)^{4/3} \left(\frac{T_\nu^4}{T_\gamma^4} \right) \quad (3)$$

At the time of CMB formation, the predicted value of N_{eff} within the SM particle content is $N_{\text{eff}}^{\text{CMB}} = 3.046$ [2], whereas the recent Planck 2018 data [4] estimates it to be $N_{\text{eff}}^{\text{CMB}} = 2.99^{+0.33}_{-0.34}$ at 95% confidence level (C.L.).

In this scenario, the Z' arising from the aforementioned $U(1)_X$ models introduces new interactions with both ν_i and e^\pm , can potentially impact the neutrino decoupling consequently altering $N_{\text{eff}}^{\text{CMB}}$. As pointed out previously, the SM particles relevant for ν_L decoupling are

⁴ By the temperature of the universe (T), we mean it as the temperature (T_γ) of the photon bath.

⁵ by ν_L we refer the whole SM neutrinos (ν_i)

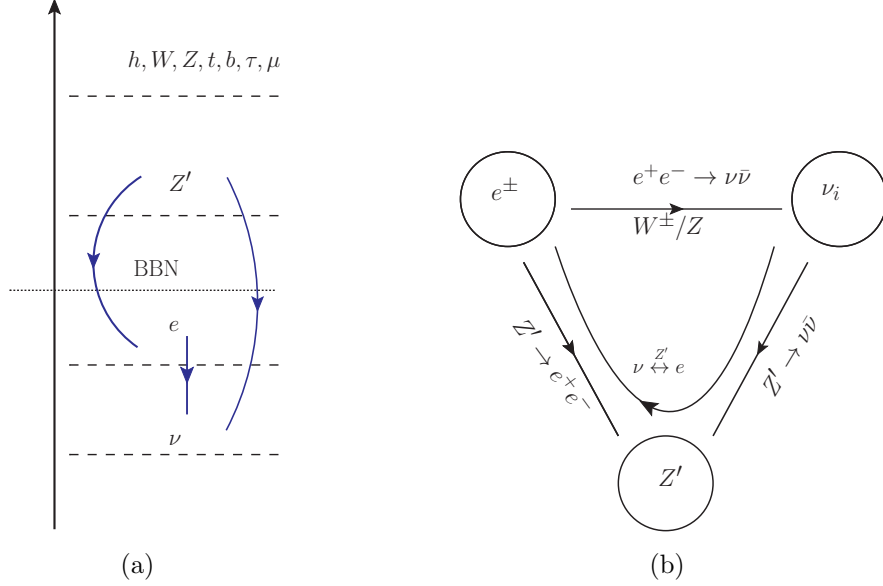


FIG. 1: Cartoon diagram of (a) particle spectrum and (b) interactions between three sectors. The vertical axis in (a) denotes the mass scale (or, temperature) and the dotted line indicates the temperature where BBN started. The blue lines in (a) signify the interactions between particles that affect N_{eff} . Here ν in the figure signify SM neutrinos (ν_i) only.

only e^\pm and ν_i , whereas the energy densities of heavy SM particles are negligible due to Boltzmann suppression. The light quarks also do not take part due to the QCD confinement at a much higher temperature around ~ 150 MeV. Following the same argument in BSM $U(1)_X$ scenario, Z' must be light enough ($M_{Z'} \lesssim \mathcal{O}(1)$ MeV) to affect ν_L decoupling which will be shown in the later part of this section. There are two other BSM particles present in our model: the BSM scalar σ and the RHN ν_R . As we elaborated in sec.2, the BSM scalar σ can be taken as heavy enough so that they are irrelevant for phenomenology at the MeV scale temperature. Hence, we integrate out σ to perceive the sole effect of light Z' in late time cosmology. And in the Majorana type mass models, ν_R are also too heavy to affect ν_L decoupling [42, 43] and we can neglect them also. However, in Dirac-type mass models, ν_R are relativistic at MeV temperature and can significantly alter N_{eff} [9]. In this work, we only consider heavy Majorana RHN and ignore their contribution to temperature evaluation. In Fig.1(a) we present the relevant mass scales by a schematic diagram.

So, in our proposed scenario, we have to trace the interactions between only three baths i.e. e, ν_L and Z' to evaluate T_ν or N_{eff} (eq.(3)). We describe the scenario using a cartoon diagram in Fig.1(b). It is essential to take care of various energy transfers among these 3 particles as they will play a key role in computing temperature evolution equations (see Appendix A). The energy transfer rates are dictated by the various collision processes and the distribution functions of respective particles [5, 44, 45]. Here we enlist the relevant processes to consider for the successful evaluation of N_{eff} .

1. **SM contributions:** The SM weak interactions are active at temperature $T \sim$ MeV.

At this point, active neutrino annihilations ($\nu_i\bar{\nu}_i \leftrightarrow e^+e^-$) as well as elastic scatterings ($\nu_i e^\pm \leftrightarrow \nu_i e^\pm$) mediated by SM Z or W^\pm take place to maintain the required thermal equilibrium of the early universe.

2. **BSM contributions to γ bath:** For a light Z' with mass $M_{Z'} \sim \mathcal{O}(\text{MeV})$ sufficient energy density can be pumped into the thermal bath via the decay and inverse decay between Z' and electrons ($Z' \leftrightarrow e^+e^-$) at temperature around $\mathcal{O}(\text{MeV})$. Additional contributions to the thermal bath may in principle come from scattering processes like $Z'Z' \leftrightarrow e^+e^-$, $Z'\gamma \leftrightarrow e^+e^-$. However, it turns out that for a very light Z' , with mass $M_{Z'} \sim \mathcal{O} \text{ MeV}$, its coupling g_X with SM fermions is highly constrained from various experimental data, $g_X \lesssim (10^{-3} - 10^{-5})$. For such a small coupling, the aforementioned decay process of Z' significantly dominates over the scattering processes. Thus we ignore the scattering contributions in our numerical calculations.
3. **BSM contributions to ν bath:** Similarly, Z' can transfer energy to ν_i bath through decay and inverse decay ($Z' \leftrightarrow \nu_i\bar{\nu}_i$) processes. Moreover, ($\nu_i\bar{\nu}_i \leftrightarrow e^+e^-$) scattering process can play an important role through one loop coupling of Z' with electron. This one-loop coupling of Z' with electrons is responsible for connecting two separate thermal baths containing ν_i and electrons. This feature can be seen in certain scenarios of the $U(1)_X$ models and we will elaborate on this issue in great detail in a later section.
4. **Within ν bath:** In this case, if we assume that different ν_i flavours have different temperatures then $\nu_i\bar{\nu}_i \leftrightarrow \nu_j\bar{\nu}_j$, ($i \neq j$) mediated by both Z and Z' will have significant impact on the overall ν thermal bath. We will address this point in detail in the last part of this section.

To construct the temperature equations and compute the energy transfer rates we adopt the formalism already developed in ref.[5, 6, 46, 47]. It is worth highlighting the approximations made in the formalism prescribed in ref.[5] before the description of temperature equations. Firstly, Maxwell Boltzmann distributions were considered to characterize the phase space distribution of all particles in equilibrium, aiding in simplifying the collision term integral. The use of the Fermi Dirac distribution in the collision term does not alter the energy transfer rates substantially [16, 48]. Additionally, the electron's mass was ignored to simplify the collision terms as non-zero electron mass would have resulted in a minimal modification of the energy transfer rate, typically less than a few percent [49]. It is to be noted that the ν_L masses can be easily neglected as the relevant temperatures for neutrino decoupling is sufficiently higher than ν_L -mass.

After successfully demonstrating all relevant processes and stating the assumptions, we are now set to construct the temperature evolution equations. The temperature equations are derived from the Liouville equation for phase space distribution of particles in a thermal bath (eq.(A1)) and the collision terms take care of the energy transfers among involved particles through the processes discussed before [50]. Following the detailed calculations of

the temperature evolution for the SM and BSM scenarios as displayed in appendices A and B, here we quote the final results of aforementioned temperature evolution equations [5, 6]:

$$\frac{dT_{\nu_L}}{dt} = - \left(4H\rho_{\nu_L} - \frac{\delta\rho_{\nu_L \rightarrow e^\pm}}{\delta t} + \frac{\delta\rho_{Z' \rightarrow \nu_L}}{\delta t} \right) \left(\frac{\partial\rho_{\nu_L}}{\partial T_{\nu_L}} \right)^{-1} \quad (4)$$

$$\frac{dT_{Z'}}{dt} = - \left(3H(\rho_{Z'} + P_{Z'}) - \frac{\delta\rho_{Z' \rightarrow \nu_L}}{\delta t} - \frac{\delta\rho_{Z' \rightarrow e^\pm}}{\delta t} \right) \left(\frac{\partial\rho_{Z'}}{\partial T_{Z'}} \right)^{-1} \quad (5)$$

$$\frac{dT_\gamma}{dt} = - \left(4H\rho_\gamma + 3H(\rho_e + p_e) + \frac{\delta\rho_{\nu_L \rightarrow e^\pm}}{\delta t} + \frac{\delta\rho_{Z' \rightarrow e^\pm}}{\delta t} \right) \left(\frac{\partial\rho_\gamma}{\partial T_\gamma} + \frac{\partial\rho_e}{\partial T_\gamma} \right)^{-1}, \quad (6)$$

where, ρ_r , P_r and T_r signify the energy density, pressure density, and temperature of species r . Terms like $\frac{\delta\rho_{a \rightarrow b}}{\delta t}$ indicate the energy transfer rate from bath a to b and is determined by integrating the collision terms (see eq.(A2)). The energy transfer rates are discussed in great detail in Appendix B. Here we assume all three ν_i generations share the same temperature T_{ν_L} ⁶ and ρ_{ν_L} is the summation over the energy densities of three generations of ν_i .

Note that, the equations in eq.(4-6) are dependent on the thermal history of heavy Z' when it remains in equilibrium with thermal bath in the early universe ($T_{Z'} \gtrsim M_{Z'}$) through its interaction with fermions (f). Z' preserves its thermal equilibrium via decay, inverse decay ($Z' \leftrightarrow f\bar{f}$) and also through scattering ($f\bar{f} \leftrightarrow Z'Z'(\gamma)$) process. Thanks to processes like $f\bar{f} \leftrightarrow Z'Z'(\gamma)$ the chemical potentials ($\mu_i(T)$) are suppressed and Z' remain in chemical equilibrium with the SM bath. The condition for the thermal equilibrium of Z' incorporates a lower bound on $g_X (\gtrsim 10^{-9})$ and the lower bound may shift slightly depending on the specific choice of $U(1)_X$ charge and the value of $M_{Z'}$. Alternatively, it is highly plausible that Z' was initially not in thermal equilibrium in the early universe, but produced from other SM particles via freeze in process. In these scenarios, it is necessary to solve the coupled equations for $\mu_i(T)$ to compute N_{eff} [7]. This alternate scenario requires a detailed complementary study which will be reported elsewhere.

As mentioned above we affix to the simplest BSM scenario assuming Z' in thermal equilibrium and set the initial condition for the set of equations eq.(4-6) as $T_{\nu_L} = T_{Z'} = T_\gamma$ at $T_\gamma \gtrsim M_{Z'}$ for the reasons already discussed before. In such case one can further simplify the scenario assuming $T_{Z'} = T_{\nu_L}$ as Z' remains coupled to ν bath for longer time than with γ bath [6]. This makes the term $\delta\rho_{Z' \rightarrow \nu_L}/\delta t = 0$ and reduces the three equations in eq.(4)-(6) into two. However, the equations described in the above format are useful for generic scenarios.

So far, we have assumed that all three ν_L share common temperature T_ν as mentioned earlier. The approximation is valid as neutrino oscillations are active around MeV temperature leading to all three generations of neutrinos equilibrating with each other[41, 51–53]. However one can also evaluate the temperatures assuming different temperatures T_{ν_i} , ($i = e, \mu, \tau$)

⁶ as for our analysis RHNs are not relevant we will often denote T_{ν_L} as T_ν

for all three generations and the relevant equation reads as (see eq.(B27)),

$$\frac{dT_{\nu_i}}{dt} = - \left(4H\rho_{\nu_i} - \left(\frac{\delta\rho_{\nu_i \rightarrow e}}{\delta t} \right)_{\text{tot}} - \sum_{j \neq i} \left(\frac{\delta\rho_{\nu_i \rightarrow \nu_j}}{\delta t} \right)_{\text{tot}} + \frac{\delta\rho_{Z' \rightarrow \nu_i}}{\delta t} \right) \left(\frac{\partial\rho_{\nu_i}}{\partial T_{\nu_i}} \right)^{-1}. \quad (7)$$

Note that earlier eq.(4) differs from the one described in eq.(7) as the later one also contains the energy transfer rate between different generations of ν_i . However the value of N_{eff} does not change significantly ($\lesssim 10\%$) if one solves the temperature equation without considering different T_{ν_i} (see Appendix C) [6]. For the same reason we stick to the simpler scenario assuming a common temperature of ν_L bath and solve eq.(4)-(6) for numerical estimation of N_{eff} throughout this paper.

After the detailed discussion of the basic framework, we are now set to perform an exhaustive numerical analysis. In Fig.2 we show case the evolution of temperature ratio (T_γ/T_ν) as well as ΔN_{eff} ($\equiv N_{\text{eff}}^{\text{CMB}} - 3.046$) with T_γ for different $U(1)_X$ charge combinations. Here we denote $T_\nu \equiv T_{\nu_i}$ with the assumption all three neutrino share a common temperature. Following the discussion in the previous paragraphs, we stress that the relevant charges for ν_L decoupling are $X_{L_i} = X_{l_i} \equiv X_i$ or more precisely their modulus values as their squared value will enter in the collision terms (see Appendix B). In the aforementioned plot, we present the simplest scenario where all 3 ν_L share the same temperature. We consider benchmark parameter (BP) values $M_{Z'} = 10$ MeV with $g_X = 10^{-7}$ (Fig.2(a) & 2(c)) and $g_X = 10^{-8}$ (Fig.2(b) & 2(d)). We will justify the importance of such a light Z' in this process at the end of this section. For such a light $M_{Z'}$ and $g_X = 10^{-7}$, we show the variation of T_γ/T_ν with T_γ and ΔN_{eff} with T_γ in Fig.2(a) and Fig.2(c) respectively. From the above figure, it is very clear that around $T_\gamma \gtrsim 10\text{MeV}$, $T_\gamma/T_\nu = 1$ as both ν_L and Z' was coupled to photon bath at that time. However, the ratio starts to increase after $T_\gamma \sim 0.5$ MeV and then saturates at low temperature ($T_\gamma \sim 10^{-2}$ MeV) as almost all the processes mentioned earlier gradually become inefficient at low T_γ . In Fig.2(c) we portray the corresponding variation in ΔN_{eff} for all the $U(1)_X$ charge combinations in Fig.2(a). As around $T_\gamma \sim 10^{-2}$ MeV the values of ΔN_{eff} become saturated we can surmise that it will remain unchanged till recombination epoch ($T_\gamma \sim 0.1$ eV) and say $\Delta N_{\text{eff}}(T_\gamma \sim 10^{-2}\text{MeV}) \equiv \Delta N_{\text{eff}}^{\text{CMB}}$. In a similar way, for $g_X = 10^{-8}$ also we display the evolution of T_γ/T_ν and ΔN_{eff} in Fig.2(b) and Fig.2(d) respectively. In Fig.2(c) and Fig.2(d) we also showcase the 2σ exclusion limit $\Delta N_{\text{eff}}^{\text{CMB}} = 0.28$ from Planck 2018 [4] and shown in black dotted line. Note that this limit is only valid at CMB and it excludes any values of ΔN_{eff} at that time above the black dotted line. It is easy to infer that in the presence of the light Z' the values differ from SM prediction. Before spelling out the physical implications of the $U(1)_X$ scenario we tabulate our findings from Fig.2 for the ease of understanding in TableII.

Both from Fig.2 and TableII it is evident that in our proposed $U(1)_X$ scenario the value of temperature ratio or $N_{\text{eff}}^{\text{CMB}}$ differs from the values predicted by SM only. One can interpret this feature from the new processes involved in ν_L decoupling apart from the SM weak

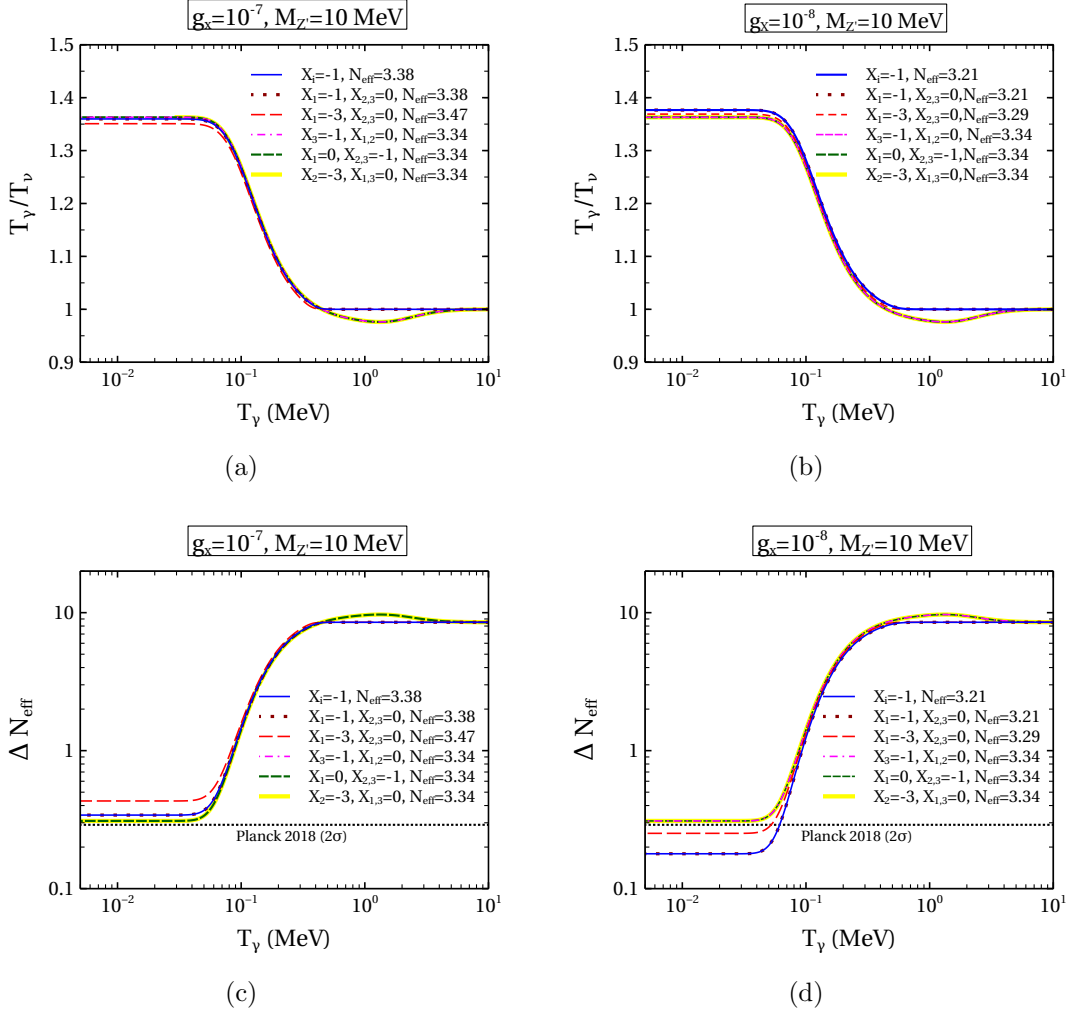


FIG. 2: Evolution of T_γ/T_ν with photon bath temperature T_γ assuming all 3 ν_L share same temperature for different $U(1)_X$ charge combinations. We chose a benchmark parameter value $M_{Z'} = 10$ MeV for both the plots. The couplings are taken $g_X = 10^{-7}$ for (a) and $g_X = 10^{-8}$ for (b). The lines corresponding to different charge combinations are indicated by the plot legends in the figure. The legends named N_{eff} in the plots refer to $N_{\text{eff}}^{\text{CMB}}$.

interactions (see Fig.1). Thus the light Z' acts as the bridge between photon and ν_L bath and tries to balance their energy densities (through decays and scatterings) and hence reduces the temperature ratio from the value predicted by the SM only. From both Fig.2(a) and Fig.2(b) we notice that for a fixed value of g_X and $X_{L_1} \neq 0$ the ratio T_γ/T_ν (at very late time) and $\Delta N_{\text{eff}}^{\text{CMB}}$ grow with an increase in $|X_1|$. For $X_1 \neq 0$ the following BSM processes affect ν_L decoupling: (i) Z' decaying to both e^+e^- and $\nu_i\bar{\nu}_i$ and (ii) scattering process $\nu_i\bar{\nu}_i \rightarrow e^+e^-$ mediated by Z' . Thus with an increase in $|X_1|$, the effective coupling (X_1g_X) governing these BSM processes increases and hence boosts the BSM contribution (see eq.(B18) and eq.(B21)). As a result, picking higher values of X_1 leads to a higher interaction rate between ν bath and photon bath leading to an enhancement in $\Delta N_{\text{eff}}^{\text{CMB}}$ or, more precisely a diminution in

$U(1)_X$ coupling	$U(1)_X$ charge			Notation	$N_{\text{eff}}^{\text{CMB}}$
	$ X_1 $	$ X_2 $	$ X_3 $		
$g_X = 10^{-7}$ Fig.2(a,c)	1	1	1	blue solid	3.38
	0	1	1	green dashed	3.34
	1	0	0	brown dotted	3.38
	0	1	0	magenta dashed dot	3.34
	0	3	0	thick yellow	3.34
	3	0	0	red dashed	3.47
$g_X = 10^{-8}$ Fig.2(b,d)	1	1	1	blue solid	3.21
	0	1	1	green dashed	3.34
	1	0	0	brown dotted	3.21
	0	1	0	magenta dashed dot	3.34
	0	3	0	thick yellow	3.34
	3	0	0	red dashed	3.29

TABLE II: Values of $N_{\text{eff}}^{\text{CMB}}$ for different $U(1)_X$ charges inferred from Fig.2.

T_γ/T_ν .

On the contrary when $X_1 = 0$ the only BSM process relevant for ν_L decoupling is $Z' \leftrightarrow \nu_{\mu,\tau}\nu_{\mu,\tau}^-$ as there is no tree level coupling of Z' with electrons. At $T_\nu < M_{Z'}$ eventually all Z' decay to ν_L transferring all their energy density to ν bath only. As all the equilibrium number density of Z' finally gets diluted to ν_L bath (with 100% branching ratio) it does not depend on the coupling strength ($X_{2/3}g_X$). There is no change in N_{eff} with the change in charge assignments (X_2, X_3) for $X_1 = 0$. For the same reason described above, we infer that for $X_1 \neq 0$, N_{eff} increases with an increase in g_X whereas with $X_1 = 0$ it does not change at all with change in g_X (comparing Fig.2(c) and Fig.2(d)). Due to the fact that for $X_1 = 0$, Z' has only decay mode to $\nu_{\mu,\tau}$, T_ν starts to increase before e^\pm decouples ($T_\gamma \sim 0.5$ MeV). This causes a slight dip in the T_γ/T_ν evolution line at higher temperature for $X_1 = 0$ in Fig.2(a) and Fig.2(b).

Before concluding the discussion about Fig.2, we point out the fact that we compute N_{eff} with a basic assumption that all ν_L share same temperature and hence all ν_L equilibrate with each other even if Z' decays (transfers energy) to any one of them. For this reason we observe similar behaviour of T_γ/T_ν for all $U(1)_X$ charge combinations with same value of X_1 and the same phenomenology elaborated in the earlier paragraph accounts for that. One should note that the $U(1)_X$ charge combination used in Fig.2 is not an exhaustive one, yet one can easily deduce the outcome of other combinations from the reasoning we made above. For example all charge combinations with $|X_1| = 1$ and $|X_2| = 0$ will lead to $N_{\text{eff}}^{\text{CMB}} = 3.38$ and 3.34 respectively for $g_X = 10^{-7}, M_{Z'} = 10$ MeV. This is the most pivotal point of our analysis and we will revisit this in the next section. At this juncture, it is worth pointing out that the dependence of $N_{\text{eff}}^{\text{CMB}}$ on g_X for $|X_i| = 0$, indicating the absence of tree-level

$Z'e^+e^-$ coupling. However, some effective coupling between Z' and e^\pm can be generated depending on the specific $U(1)_X$ model [6]. In the subsequent section, we will extensively discuss such a scenario where the induced $Z'e^+e^-$ coupling plays a crucial role in deciding $N_{\text{eff}}^{\text{CMB}}$. For the ease of our notation from now on whenever we say N_{eff} , we refer to $N_{\text{eff}}^{\text{CMB}}$ only.

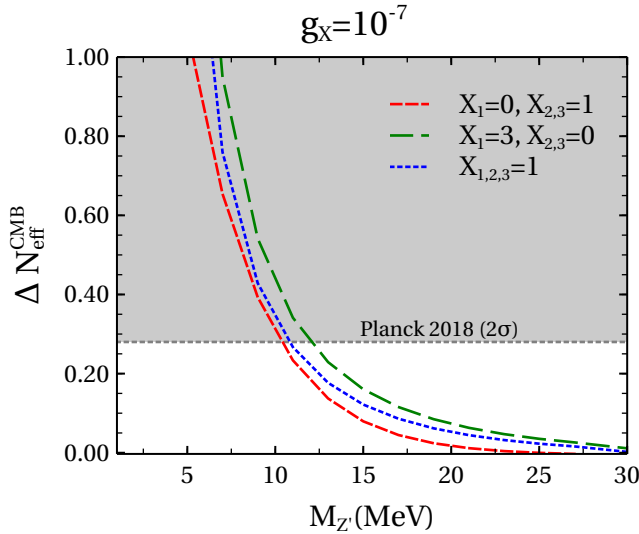


FIG. 3: Variation of $\Delta N_{\text{eff}}^{\text{CMB}}$ with $M_{Z'}$ assuming all three ν_L share same temperature for different $U(1)_X$ charge combinations. We choose a fixed value of $g_X = 10^{-7}$.

Having discussed the dependence of N_{eff} on the two most important parameters of the BSM model: the Z' universal gauge coupling g_X and $U(1)_X$ charge combinations, now we turn our attention to investigate its dependence on the light $M_{Z'}$. In Fig.3 we show variation of $\Delta N_{\text{eff}}^{\text{CMB}}$ ⁷ with $M_{Z'}$ for a fixed coupling $g_X = 10^{-7}$ with different $U(1)_X$ charge combinations. Rather than showing all the $U(1)_X$ charge combinations used in Fig.2, we just portray only three distinct combinations of them in Fig.3. We indicate the combinations ($|X_{1,2,3}| = 1$), ($|X_1| = 0, |X_{2,3}| = 1$), and ($|X_1| = 3, |X_{2,3}| = 0$) by blue, green and red lines respectively. From the aforementioned figure, we observe that $\Delta N_{\text{eff}}^{\text{CMB}}$ decreases as $M_{Z'}$ increases and eventually it becomes almost zero, reproducing the SM value of N_{eff} when $M_{Z'} \gtrsim 30$ MeV. This feature can be interpreted from our previous discussion in the context of Fig.1. The energy density of heavier Z' gets Boltzmann suppressed at ν_L decoupling temperature ($T_\gamma \sim 2$ MeV) making the BSM contribution less significant in deciding ν_L decoupling. On the other hand Z' mediated scattering processes between ν and e , also propagator suppressed for higher $M_{Z'}$. At very high $M_{Z'}$ ($\gtrsim 30$ MeV), the BSM contribution hardly plays any role in deciding ν_L decoupling resulting $\Delta N_{\text{eff}}^{\text{CMB}} = 0$. Following the same

⁷ To amplify the change in N_{eff} with $M_{Z'}$ and portray more lucidly, for this particular plot we switch to $\Delta N_{\text{eff}}^{\text{CMB}} \equiv N_{\text{eff}} - 3.046$. The variation in N_{eff} will immediately follow from it.

argument we infer that a lower value of $M_{Z'}$ will enhance the BSM contribution and hence $\Delta N_{\text{eff}}^{\text{CMB}}$. For a fixed value of $M_{Z'}$, the difference in $\Delta N_{\text{eff}}^{\text{CMB}}$ for different $U(1)_X$ charge combinations can be easily apprehended from the discussion in the context of Fig.2. So far we explored the dependence of $\Delta N_{\text{eff}}^{\text{CMB}}$ on various model parameters, and the dependence of N_{eff} also can be easily understood from that. Keeping in mind the key findings from $U(1)_X$ Z' models in the context of N_{eff} , in the following section we will explore their contribution to alleviating the Hubble tension.

4. NUMERICAL RESULTS

In the previous section, we pinned down the key aspects of light Z' from generic $U(1)_X$ extension and showed that the $U(1)_X$ charge assignments play a key role in deciding N_{eff} as well as its dependence on coupling g_X . In this section, we will take a closer look at the model parameters and explore their cosmological implication through exhaustive numerical scans. Though one can have numerous $U(1)_X$ charge assignments as suggested in the Table I., in the context of N_{eff} the arbitrary charge assignments can be categorised into only two classes when we assume all ν_L share the same temperature (through oscillation). Needless to say, it is the coupling of Z' with electron (apart from ν_i) that affects the N_{eff} and not the couplings with τ, μ or quarks, for the reasons already discussed earlier. Thus the light Z' models can be broadly classified into two pictures: $X_1 \neq 0$ and $X_1 = 0$, more precisely, whether Z' has coupling with electron or not (see Fig.4).

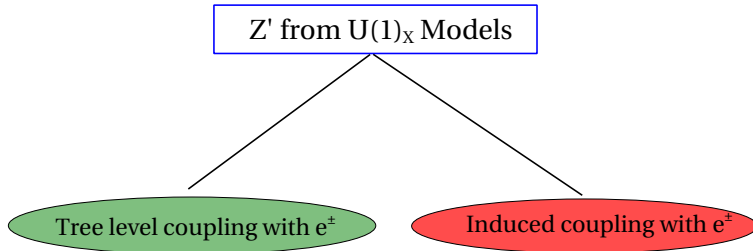


FIG. 4: Classification of Z' models depending on $X_1 = 0$ and $X_1 \neq 0$

In our discussions on the light Z' phenomenology so far we have mainly focused on its tree level couplings with fermions. Yet, it is important to highlight that even in the absence of tree level $Z'e^+e^-$ interaction ($X_1 = 0$), Z' can develop induced coupling⁸ with e^\pm [54]. As a result, for $|X_1| = 0$, while computing N_{eff} , we need to consider the following effective $Z'e^+e^-$ interaction Lagrangian:

$$\mathcal{L}_{int} = (\epsilon e) \bar{e} \gamma^\mu e Z'_\mu, \quad (8)$$

⁸ The source of the induced coupling is model dependent. It can originate from kinetic mixing, can be loop induced or can originate from flavor violating couplings. In this model independent section we will remain agnostic about its origin.

where ϵ is the induced effective coupling. If, for instance, the induced coupling is generated from the $\gamma - Z'$ kinetic mixing at one loop level, its expression is given as (see Appendix A of ref. [54]).

$$\epsilon = \frac{g_X}{2\pi^2} \sum_{\ell} X_{\ell} \int_0^1 dx x(1-x) \log\left(\frac{\Lambda^2}{\Delta_{\ell}}\right), \quad (9)$$

where, $\Delta_{\ell} = m_{\ell}^2 - x(1-x)q^2$, Λ denotes an arbitrary mass scale and the summation includes all $U(1)_X$ charged fermions with mass m_{ℓ} . This induced coupling will have a significant impact in scenarios where $X_1 = 0$, as we'll shortly discover. While we aim to maintain a model-independent discussion, the effective coupling described in eq.(8) relies on the characteristics of particular $U(1)_X$ models. Therefore, to compare our findings with existing literature, we opt for the benchmark value of the effective coupling, setting $\epsilon = -\frac{g_X}{70}$, which is very commonly used for $L_{\mu} - L_{\tau}$ models (with $X_1 = 0$)[6, 55]. Henceforth, in all our numerical results, we will use this particular value of ϵ .

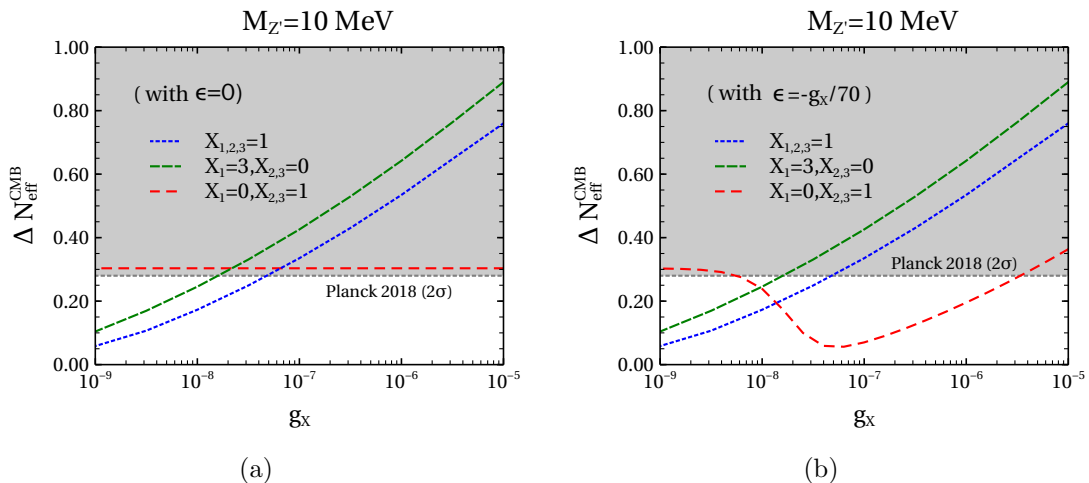


FIG. 5: Variation of $\Delta N_{\text{eff}}^{\text{CMB}}$ with g_X in (a) with $\epsilon = 0$ and in (b) with $\epsilon = -\frac{g_X}{70}$ assuming all 3 ν_L share same temperature for different $U(1)_X$ charge combinations. We choose a fixed value of $M_{Z'} = 10$ MeV for both (a) and (b).

In Fig.5, we aim to investigate the role of g_X on $\Delta N_{\text{eff}}^{\text{CMB}}$ while maintaining a constant $M_{Z'} = 10$ MeV and as stated earlier the variation of N_{eff} also follows from it. This scrutiny involves two distinct scenarios for the $Z'e^+e^-$ coupling: (a) solely with tree-level couplings ($\epsilon = 0$) depicted in Fig.5(a), and (b) considering induced coupling as well ($\epsilon \neq 0$) shown in Fig.5(b). We display the variation of $\Delta N_{\text{eff}}^{\text{CMB}}$ with g_X for three $U(1)_X$ charge combinations ($|X_{1,2,3}| = 1$), ($|X_1| = 0, |X_{2,3}| = 1$) and ($|X_1| = 3, |X_{2,3}| = 0$) by blue, green and red lines respectively. In both Fig.5(a) and Fig.5(b), the grey band corresponds to the value of $\Delta N_{\text{eff}}^{\text{CMB}}$ that is excluded by the 2σ upper limit obtained from the Planck 2018 measurement [4]. Note that the dependence of $\Delta N_{\text{eff}}^{\text{CMB}}$ (and hence N_{eff}) on g_X for the cases with $X_1 \neq 0$ remains the same even after including mixing. This feature is easy to realize as the $Z'e^+e^-$

induced coupling (ϵ) is suppressed by an order of magnitude compared to the corresponding Ze^+e^- tree level interaction. Hence, in the presence of the tree-level $Z'e^+e^-$ interaction ($X_1 \neq 0$), one can easily ignore the contribution of Z' arising due to the induced coupling ϵ . For the reasons already discussed in sec.3, the BSM contribution increases as the values of g_X rise, leading to an increase in $\Delta N_{\text{eff}}^{\text{CMB}}$ (also N_{eff}) also, as shown in the aforementioned figure.

However, comparing Fig.5(a) and Fig.5(b) one notices that the dependence $\Delta N_{\text{eff}}^{\text{CMB}}$ on g_X for the case with $X_1 = 0$ changes drastically when the induced coupling ($\epsilon \neq 0$) is present. In Fig.5(a), we discern that $\Delta N_{\text{eff}}^{\text{CMB}}$ remains unchanged with variations in g_X for $X_1 = 0$ in the absence of induced coupling ($\epsilon = 0$). In this scenario, regardless of the associated coupling, the Z' decay is limited to ν_L exclusively, transferring its entire energy density, as reasoned in sec.3. This observation upholds our earlier analysis discussed in the preceding section. On the other hand, when $|X_1| = 0$, in the presence of the induced coupling ($\epsilon \neq 0$), Z' can couple to e^\pm . Thus for a nonzero ϵ the decay $Z' \rightarrow e^+e^-$ and $\nu_i\bar{\nu}_i \rightarrow e^+e^-$ scattering processes mediated by Z' continue during ν_L decoupling temperature ($T_\gamma \sim 1$ MeV). Among these two processes, the scattering process tries to balance e and ν_L bath by increasing T_ν or increasing N_{eff} . Therefore, as g_X increases, the contribution of BSM scenarios also increases, resulting in an overall rise in $\Delta N_{\text{eff}}^{\text{CMB}}$. This feature is reflected in Fig.5(b) (red line) for $g_X \gtrsim 4 \times 10^{-8}$. On the other extreme, for $g_X \lesssim 4 \times 10^{-8}$, the scattering process ($\propto \epsilon^2 g_X^2$) is unable to compete with the tree level decay $Z' \rightarrow \nu_L\bar{\nu}_L$ ($\propto g_X^2$) process. Hence, for lower values of g_X ($\lesssim 4 \times 10^{-8}$), Z' promptly decays to ν bath transferring all its energy to ν sector and the scattering processes become inefficient to dilute this extra energy density to e bath. So, when g_X ($\lesssim 4 \times 10^{-8}$) we see a distinct rise in $\Delta N_{\text{eff}}^{\text{CMB}}$ for $X_1 = 0$ in Fig.5(b). When g_X ($\lesssim 7 \times 10^{-8}$) is very small, the BSM contribution that affects the evolution of the energy density of ν_L is primarily dominated by Z' decay processes. Irrespective of the coupling, at this level, the Z' particle transfers all its energy density to ν_L . It is essential to note that at this point, the value of $\Delta N_{\text{eff}}^{\text{CMB}}$ for $X_1 = 0$ turns out to be identical for both scenarios with and without induced coupling when comparing Fig.5(a) and Fig.5(b). This outcome serves as validation for our previous argument. At this point, it is worth pointing out another aspect of this tree-level vs induced Z' coupling in generating non-zero contributions of BSM physics to $\Delta N_{\text{eff}}^{\text{CMB}}$. When g_X exceeds 10^{-8} and $X_1 = 0$, the other two $U(1)_X$ charge combinations with non-zero $|X_1|$ result in the tree-level $Z'e^+e^-$ interaction yielding greater contributions to $\Delta N_{\text{eff}}^{\text{CMB}}$ compared to the aforementioned induced Z' coupling. This distinction is particularly noticeable in Fig. 5(b).

Now, we put forward the main thrust of this paper and split the analysis of light Z' realized in different $U(1)_X$ models in the context of N_{eff} into two categories as shown in Fig.4. The consequences of all other $U(1)_X$ charge combinations can be easily anticipated from the broad classifications. Following this line of thought we will now perform numerical scans to explore the imprints in N_{eff} in the presence of light Z' emerging from two broad classes of generic $U(1)_X$ models in the following two subsections.

4.1. Z' having tree level coupling with e^\pm

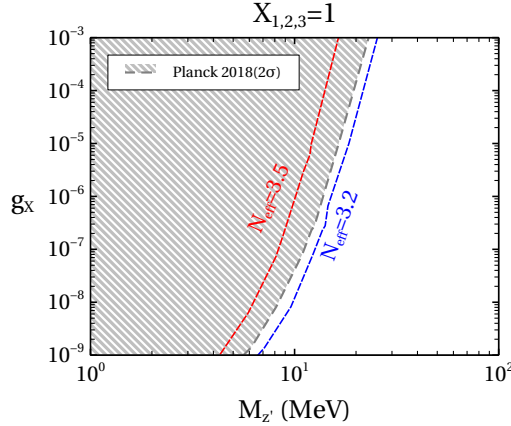


FIG. 6: The parameter space for N_{eff} is depicted in the $M_{Z'}$ vs. g_X plane for a generic $U(1)_X$ gauge extension with the charge assignment $|X_{1,2,3}| = 1$. The 2σ upper bound from Planck 2018 [4] is depicted by the grey dashed line, excluding the parameter space to the left of that line shown by the grey region. The blue and red dashed lines indicate the values of $N_{\text{eff}}^{\text{CMB}} = 3.2$ and 3.5 , respectively, where the H_0 tension can be relaxed as pointed out in ref.[30].

Here we consider the charge assignment $|X_{1,2,3}| = 1$ and show the contours of constant N_{eff}^9 in $M_{Z'}$ vs. g_X plane in Fig.6. In the same plot, we also showcase the 2σ bound from Planck 2018 data [4] shown by the grey dashed line. The parameter space to the left of the grey dashed line, as shown by the grey region, is excluded by Planck 2018 data at 2σ [4]. From the figure we observe that for a fixed g_X , N_{eff} decreases with an increase in $M_{Z'}$ as we explained in the context of Fig.3. For very high $M_{Z'}$ the contribution to N_{eff} becomes negligible. We consider the lowest value of $g_X = 10^{-9}$ as below that, Z' fails to thermalize in the early universe. Following the discussion made earlier in this section, it is evident that increasing the value of $|X_1|$ will lead to a gradual shift of the contour for Planck 2018 upper limit (grey dashed line) towards right i.e. towards higher values of $M_{Z'}$.

4.2. Z' having induced coupling with e^\pm

Here we consider the following charge assignment $|X_1| = 0, |X_{2,3}| = 1$ and show the contours of constant N_{eff} in $M_{Z'}$ vs. g_X plane in Fig.7. Similar to Fig.6 we portray the contour lines for $N_{\text{eff}} = 3.2$, $N_{\text{eff}} = 3.5$ and 2σ upper limit from Planck 2018 [4] depicted by blue, red and grey dashed lines. The grey region to the left of the grey dashed line in each figure is excluded by the 2σ upper bound from Planck 2018 data [4].

⁹ As stated earlier by N_{eff} we refer N_{eff} at the time of CMB.

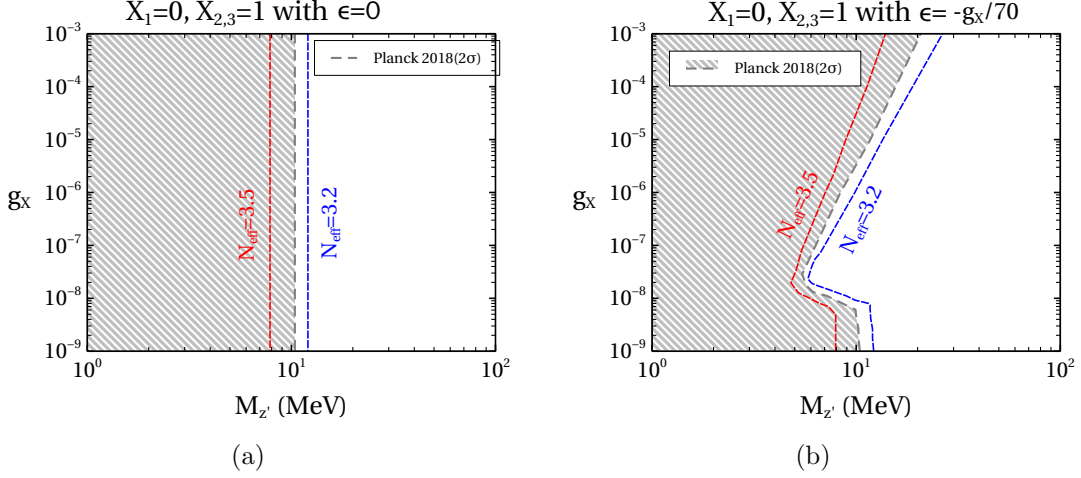


FIG. 7: Parameter space space for N_{eff} in $M_{Z'}$ vs. g_X plane for a generic $U(1)_X$ gauge extension with the charge assignment $|X_1| = 0, |X_{2,3}| = 1$. We show the results without kinetic mixing ($\epsilon = 0$) in (a) and with kinetic mixing ($\epsilon \neq 0$) in (b). The grey dashed line in each figure represents the 2σ upper bound from Planck 2018 [4], excluding the parameter space to its left, as depicted by the grey region. The blue and red dashed lines in each figure denote $N_{\text{eff}}^{\text{CMB}}$ values at 3.2 and 3.5, respectively, indicating the intermediate regions where the H_0 tension can be relaxed [30].

We show the numerical results for the case $|X_1| = 0$ without induced coupling ($\epsilon = 0$) in Fig.7(a). The dependence of N_{eff} on the model parameter g_X is pretty straight forward as we noticed in earlier Fig.5(a). For $|X_1| = 0$, in the absence of induced coupling, N_{eff} stays unchanged despite the variation in g_X , resulting in distinct vertical lines of N_{eff} contours in $M_{Z'} - g_X$ plane in Fig.7(a). Also, from the same figure we note a decrease in N_{eff} with an increase in $M_{Z'}$ for a fixed g_X , as elaborated earlier. Note that, in the absence of induced coupling ($\epsilon = 0$) the contour for Planck 2018 upper limit (grey dashed line) will not change with increasing $X_{2,3}$ for such kind ($X_1 = 0$) of $U(1)_X$ models as argued before in context of Fig.5(a).

However, the results are quite different after including the induced coupling ($\epsilon \neq 0$) of Z' with electrons as shown in Fig.7(b). Due to the induced coupling of Z' with electrons, the N_{eff} contours replicate the feature of the $|X_1| = 1$ case (as shown in Fig.6) for higher values of g_X ($\gtrsim 10^{-8}$) with a knee like pattern around $g_X \sim 10^{-8}$. Such non-trivial dependence is the consequence of the interplay between tree-level decay ($Z' \rightarrow \nu_L \bar{\nu}_L$) and the induced Z' mediated scattering as explained earlier in detail. We notice the bend in the contour lines in Fig.7(b) since the collision term accounting for the BSM contribution in computing N_{eff} is decay dominated in lower coupling region ($g_X \lesssim 4 \times 10^{-8}$). It is worth mentioning that for $\epsilon \neq 0$ the contour for Planck 2018 upper limit (grey dashed line) will shift towards right with increasing $X_{2,3}$ for $g_X \gtrsim 4 \times 10^{-8}$ and will remain unchanged for $g_X \lesssim 4 \times 10^{-8}$.

Thus from this section, we propound that the cosmological imprints of light Z' models due to different charge assignments leading to different $U(1)_X$ models can be put under

the same roof following our prescription. However, in the model independent analysis, we ignored the experimental constraints which are inevitably relevant for our parameter space. The detail analysis of those constraints on light Z' depends on specific $U(1)_X$ choice and will be reported elsewhere [56]. For completeness, we will show the numerical results for some specific $U(1)_X$ models along with experimental constraints in the next section.

5. SPECIFIC $U(1)_X$ SYMMETRIES: $U(1)_{B_3-3L_j}$

Let's now look at the type of $U(1)_X$ symmetry where the symmetry is flavour dependent in both quarks as well as the lepton sector namely the $U(1)_{B_3-3L_j}$ gauge symmetries [22]. In this case, we will consider the following three gauged $U(1)$ symmetries: $U(1)_{B_3-3L_e}$, $U(1)_{B_3-3L_\mu}$ and $U(1)_{B_3-3L_\tau}$.

The charges of three of such symmetries are listed in Table III. The charges of the other $U(1)_{B_3-3L_j}$ symmetries are analogous and can be similarly written without difficulty.

Fields	$SU(3)_c \times SU(2)_L \times U(1)_Y$	$U(1)_{B_3-3L_1}$	$U(1)_{B_3-3L_2}$	$U(1)_{B_3-3L_3}$
Q_i	$(3, 2, \frac{1}{3})$	$(0, 0, 1)$	$(0, 0, 1)$	$(0, 0, 1)$
u_i	$(3, 1, \frac{4}{3})$	$(0, 0, 1)$	$(0, 0, 1)$	$(0, 0, 1)$
d_i	$(3, 1, -\frac{2}{3})$	$(0, 0, 1)$	$(0, 0, 1)$	$(0, 0, 1)$
L_i	$(1, 2, -1)$	$(-3, 0, 0)$	$(0, -3, 0)$	$(0, 0, -3)$
l_i	$(1, 1, -2)$	$(-3, 0, 0)$	$(0, -3, 0)$	$(0, 0, -3)$
ν_{R_i}	$(1, 1, 0)$	(x_1, x_2, x_3)	(x_1, x_2, x_3)	(x_1, x_2, x_3)
Φ	$(1, 2, 1)$	0	0	0
σ	$(1, 1, 0)$	y	y	y

TABLE III: Particle content and $U(1)_{B_3-3L_j}$ gauge charge assignments of Standard Model and new particles. The charges of ν_{R_i} can be fixed by anomaly cancellation condition while the charge of σ depends on the details of the nature and model for neutrino mass generation.

For all three cases, the charges of ν_{R_i} can be fixed by the anomaly cancellation conditions. A convenient anomaly free charge assignment for ν_{R_i} is $\nu_{R_i} = -3, \nu_{R_j} = 0; j \neq i$ for the $U(1)_{B_i-3L_j}$ symmetry e.g. for say $U(1)_{B_3-3L_2}$ gauge symmetry the charges can be $\nu_R \sim (0 - 3, 0)$ [22]. The charges of the σ field depend on the details of the model and we will not go into details of the model building unless needed¹⁰. And as we mentioned earlier in sec.3, we assume this ν_{R_i} and σ to be heavy enough that they are irrelevant for the analysis of N_{eff} .

Before exploring the phenomenology of the specific $U(1)_X$, we would like to outline an overview of the exclusion bounds on the mass of the light-gauge boson ($M_{Z'}$) and

¹⁰ see for example ref.[22]

corresponding gauge coupling (g_X) within the mass range $M_{Z'} \sim \mathcal{O}(10)$ MeV, which is our point of interest. Here, we will briefly review various types of low-energy experimental observations that can be used to constrain the scenarios involving any $U(1)_X$. In the following subsections, we will present the exclusion bound identified by each low-energy experiment for a specific $U(1)_{B_3-3L_i}$ scenario ($i = e, \mu, \tau$), along with our cosmological findings.

Elastic electron-neutrino scattering (E ν ES): The elastic scatterings of neutrinos with electrons ($\nu_\alpha e \rightarrow \nu_\alpha e$, $\alpha = e, \mu, \tau$) in laboratory experiments serve as one of the probes for non-standard interaction of neutrino and electron with the light-gauged boson (Z'). In SM, the $e - \nu_e$ scattering involves both charged-current (CC) and neutral-current (NC) weak interactions, whereas $e - \nu_{\mu, \tau}$ scattering is solely governed CC interaction [28]. The elastic $e - \nu_{e, \mu, \tau}$ scattering can be altered in the presence of an additional NC interaction mediated by the $U(1)_X$ gauge boson Z' , which can be probed in the low-energy scattering experiments. Note that the interference terms in the matrix amplitude between the SM (W and Z-mediated) and BSM (Z' -mediated), play a critical role in altering the scattering rate. The interference term in differential cross section is given by [54],

$$\left[\frac{d\sigma_{i-e}}{dE_R} \right]_{\text{Interference}} = \frac{\sqrt{2}G_F m_e}{\pi} \left(\frac{(g_X X_1)(g_X X_i)}{(2E_R m_e + M_{Z'}^2)} \right) \times \left[(g_L^i + g_R^i) \left(1 - \frac{m_e E_R}{2E_\nu^2} \right) - g_R^i \frac{E_R}{E_\nu} \left(2 - \frac{E_R}{E_\nu} \right) \right], \quad (10)$$

where E_R and E_ν denote electron recoil energy and incoming neutrino energy respectively. $g_{L,R}$ is defined in appendix A. For the cases where $X_1 = 0$ the term $(g_X X_1)$ will be replaced by ϵe in eq.(10). Thus observing the electron recoil rate imposes constraints on the $M_{Z'} - g_X$ plane for a model-specific scenario. The coupling strength of the light gauge boson with leptons varies over gauge extensions. As a result, the constraints will vary from model to model.

Borexino [19] and dark matter experiments like XENON 1T [57] dedicated to measuring the electron recoil rate, can be relevant in the context of $e - \nu_\alpha$ elastic scattering [20]. The Borexino experiment is designed to study the low-energy solar neutrinos (ν_e)¹¹ produced via decay of ${}^7\text{Be}$ by observing the electron recoil rate through the neutrino-electron elastic scattering process [20]. These solar neutrinos undergo flavour change as they travel from the sun to the detector. This flavor changing phenomena $\nu_e \rightarrow \nu_\alpha$ ($\alpha = e, \mu, \tau$) can be accounted using the transition probability $P_{e\alpha}$ [58]. Therefore the number of events for solar neutrinos (ν_e) interacting with the electrons in the Borexino will be $N_{\nu_e} \propto \sum_{\alpha=e, \mu, \tau} P_{e\alpha} \sigma_{e-\nu_\alpha}$ [28, 58]. Note that in Solar neutrino flux $P_{ee} (\sim 50\%) > P_{e\mu} = P_{e\tau}$ and the dominant contribution in interference term is due to ν_e as it has both CC and NC interaction with electron [28].

¹¹ E ν ES event rates for atmospheric neutrinos are negligible compared to solar ones [20].

Hence for $X_1 \neq 0$ one can approximate the differential recoil rate [28],

$$\left[\frac{dR}{dE_R} \right]_{\text{BSM}} \propto P_{ee} \left[\frac{d\sigma_{ee}}{dE_R} \right]_{\text{Interference}} \quad (11)$$

Note that when $X_1 = 0$ i.e. in the absence of tree-level coupling of Z' with electron one has to consider the elastic scattering (via loop induced coupling with Z') of an electron with $\nu_{\mu/\tau}$ with specific transition probabilities.

Coherent elastic neutrino-nucleus scattering (CE ν NS): The COHERENT experiment investigates coherent elastic scattering between neutrinos and nucleus in CsI material ($\nu N \rightarrow \nu N$) [29, 55, 59]. This mode of interaction opens up new opportunities for studying neutrino interactions, including the introduction of a new light gauge boson in this case. In SM, the elastic neutrino-nucleus scattering ($\nu - N$) takes place via the NC interactions between neutrinos ($\nu_{e,\mu,\tau}$) and nucleons or more precisely with the first generation of quarks ($q = \{u, d\}$). The additional NC interaction introduced by the light gauge boson Z' of $U(1)_X$ can contribute to the CE ν NS process. The modification to SM CE ν NS, due to the Z' can be utilized to constrain the parameter space of $M_{Z'}$ vs g_X plane. Similar to E ν ES, the exclusion limit is also dependent on the specific gauged scenarios. This is because the coupling strength of quarks and neutrinos with the light-gauged boson is influenced by the specific gauge choice. However, in contrast to E ν ES experiment, CE ν NS is lepton flavor independent and one has to consider interaction with all 3 ν . For a detailed discussion see ref.[20].

Supernova 1987A (SN1987A): Non-standard neutrino interactions with a light gauge boson can also affect the cooling of core-collapse supernovae (SN) which is a powerful source of neutrinos (ν_e) [40, 60]. The non-standard neutrino interaction gives rise to the initial production of light-gauged bosons in the core of a supernova (SN), $\nu_\alpha \bar{\nu}_\alpha \rightarrow Z'$, resulting in energy loss in the SN core [6]. After production the late decay of these Z' into neutrinos ($Z' \rightarrow \nu_i \bar{\nu}_i$) has the potential to modify the neutrino flux emitted by the SN [40]. Additionally, the neutrino self-interactions mediated by the light Z' may also affect energy loss in the SN core [61]. Thus the observation of the SN 1987A neutrino burst imposes constraints on these interactions [62]. However, there can be additional processes that might place stronger constraints from SN 1987A on light Z' models [63] and explicit derivation of that is beyond the scope of this work.

Neutrino trident: The neutrino trident production mode, in which neutrinos interact with a target nucleus to produce a pair of charged leptons without changing the neutrino flavor ($\nu N \rightarrow \nu N \mu^+ \mu^-$), is a powerful tool for probing new physics [64]. The gauge extension introduces new interactions between leptons and light gauge bosons, increasing the rate of neutrino trident production, as predicted by the SM. Therefore any gauge extended scenarios associated with muon ($X_2 \neq 0$) face constraints from existing

neutrino trident production experimental results [22].

After having a generic discussion on the constraints relevant to our analysis, in the following two subsections we present our numerical results for specific $U(1)_X$ gauge choice. We portray the bound from N_{eff} on these models along with the constraints discussed above. In the same plane, we also indicate the parameter space that can relax the H_0 tension.

5.1. Gauged $U(1)_{B_3-3L_e}$ symmetry

In this subsection we show the values of N_{eff} for light Z' in $U(1)_{B_3-3L_e}$ gauge extension. We show our numerical results in $M_{Z'}$ vs. g_X plane in Fig.8. In the same plane, we also portray other relevant astrophysical and experimental constraints. The grey dashed line in the same plot signify the 2σ upper limit on N_{eff} from Planck 2018 data [4]. It excludes the parameter space to the left of that line as shown by the grey shaded region. One can easily infer from the figure that for a fixed g_X with increasing $M_{Z'}$ the value of N_{eff} decreases which is explained in detail in the previous section. Note that for $U(1)_{B_3-3L_e}$, Z' has tree level coupling with e^\pm ($X_1 = -3$) and hence it belongs to the group of $U(1)_X$ models with $|X_1| \neq 0$ following our discussion in previous section 4.1. For this, we notice that the behavior of N_{eff} with g_X is similar to what we observed in the context of Fig.6. However, for $U(1)_{B_3-3L_e}$ model $|X_1| = 3$ and hence for fixed g_X and $M_{Z'}$ the value of N_{eff} will be higher compared to the case considered in Fig.6 for the reason already elaborated before. As a result we notice the N_{eff} lines in Fig. 8 has moved rightwards compared to Fig.6.

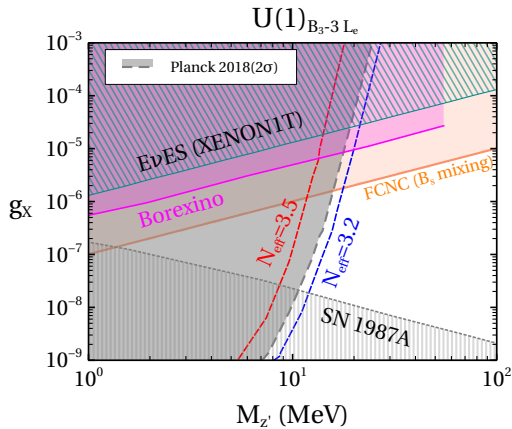


FIG. 8: Constraints from cosmology and low energy experiments in $M_{Z'}$ vs. g_X plane for a generic $U(1)_{B_3-3L_e}$ gauge extension. The 2σ upper bound from Planck 2018 [4] is shown by the grey dashed line and it excludes the parameter space to the left side of that line as shown by the grey shaded region. The region between the $N_{\text{eff}} = 3.2$ (blue dashed) and $N_{\text{eff}} = 3.5$ (red dashed) lines helps relax the H_0 tension, as mentioned in the ref. [30].

In the same plane in Fig.8 we showcase the relevant phenomenological constraints that we mentioned earlier. Since Z' has tree level coupling with electron in $U(1)_{B_3-3L_e}$ model, it

attracts strong constraint from E ν ES [20]. The exclusion region from E ν ES with XENON1T experiment is shown by the region shaded by dark cyan diagonal lines. In a similar fashion, Borexino also constrains the parameter space shown by the magenta shaded region [20]. In $U(1)_{B_3-3L_e}$ model the light Z' has no tree-level coupling with the first two generations of quarks $(u, d), (c, s)$ which is important for CE ν NS. However, Z' can have induced coupling with first-generation quarks via CKM mixing [22] and can contribute to CE ν NS. In SM the CKM matrix V_{CKM} is constructed from charge current interaction between quarks [65],

$$J_W^\mu = (\bar{q}_u)_L \mathcal{U}_L \gamma^\mu \mathbb{I}_{3 \times 3} \mathcal{D}_L^\dagger (q_d)_L \quad (12)$$

where, $q_u \equiv (u \ c \ t)^\dagger$ and $q_d \equiv (d \ s \ b)^\dagger$. \mathcal{U}_L and \mathcal{D}_L are rotation matrices that diagonalize mass matrices for q_u and q_d respectively. The CKM matrix can be constructed as $V_{\text{CKM}} = \mathcal{U}_L \mathcal{D}_L^\dagger$ [65]. For our estimation we take $\mathcal{U}_L = \mathbb{I}$ and hence $\mathcal{D}_L = V_{\text{CKM}}^\dagger$ [22]. In our scenario as Z' couples to only third generation of quarks (with $\mathcal{L}_{\text{int}} \supset g_X J_{Z'}^\mu Z'_\mu$) it may induce flavor changing neutral current (FCNC) and the Noether current ($J_{Z'}^\mu$) is given by,

$$J_{Z'}^\mu = (\bar{q}_d)_L \mathcal{D}_L \gamma^\mu \begin{pmatrix} 0 & 0 & 0 \\ 0 & 0 & 0 \\ 0 & 0 & 1 \end{pmatrix} \mathcal{D}_L^\dagger (q_d)_L. \quad (13)$$

After inserting the values of the elements of \mathcal{D}_L matrix [66], in eq.(13) the Z' effective coupling with d quark takes the following form:

$$\mathcal{L} \supset (0.006 \ g_X) Z'_\mu \bar{d}_L \gamma^\mu d_L \quad (14)$$

Using this we translate the bound from CE ν NS experiment in our scenario and obtain that it excludes the parameter space for $g_X \gtrsim 10^{-2}$. This limit is weaker than E ν ES and hence not shown in Fig.8. As Z' has coupling with b quark it generates $B_s - \bar{B}_s$ mixing and hence it attracts constraint indicated by orange shaded region [22]. Finally, the bound from supernova cooling is shown by the region shaded with grey vertical lines [6].

5.2. Gauged $U(1)_{B_3-3L_\mu}$ symmetry

In this subsection, we present our analysis with N_{eff} for a light Z' in the gauged extension of $U(1)_{B_3-3L_\mu}$. Analogous to the previous subsection we show our numerical results in $M_{Z'}$ vs. g_X plane in Fig.9 along with all relevant astrophysical and experimental constraints. The grey dashed line in the same plot signify the 2σ upper limit on N_{eff} from Planck 2018 data [4] and likewise before. The grey shaded region depicts the exclusion of the parameter space to the left of the grey dashed line.

However, unlike previous scenario, for $U(1)_{B_3-3L_\mu}$, Z' has no tree level coupling with e^\pm

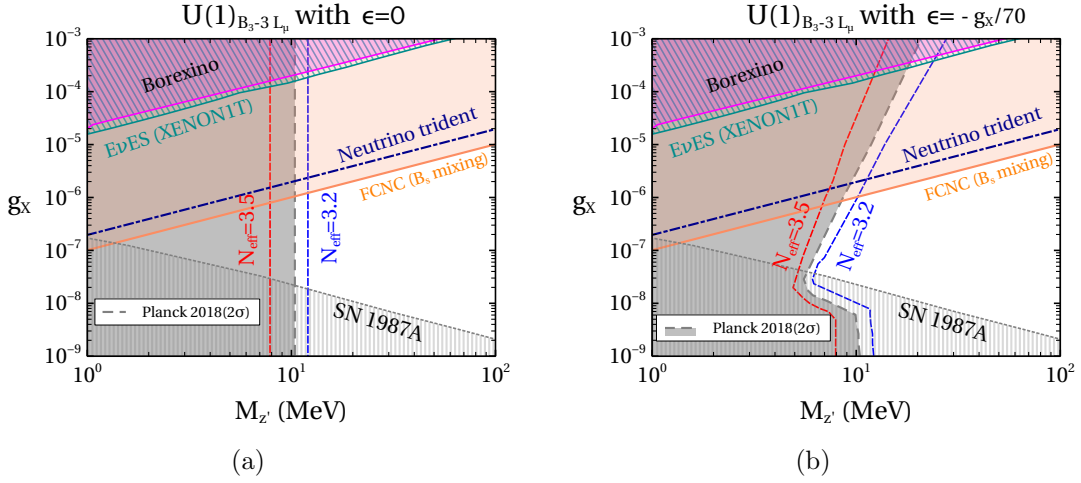


FIG. 9: Constraints from cosmology and low energy experiments in $M_{Z'}$ vs. g_X plane for a generic $U(1)_{B_3-3L_\mu}$ gauge extension. We present the results without loop induced mixing ($\epsilon = 0$) in (a) and with loop induced mixing ($\epsilon \neq 0$) in (b). The grey dashed line represents the 2σ upper bound from Planck 2018 [4], excluding the parameter space on the left side of the line as shown by the grey shaded region. The region between the blue dashed line ($N_{\text{eff}} = 3.2$) and the red dashed line ($N_{\text{eff}} = 3.5$) indicates the parameter space where the H_0 tension can be relaxed as mentioned in ref.[30].

($X_1 = 0$) and hence it belongs to other class of $U(1)_X$ models with $|X_1| = 0$ as discussed in previous sub-section 4.2. We present our numerical results with the two values of effective coupling, $\epsilon = 0$ and $\epsilon = -g_X/70$ in Fig.9(a) and Fig.9(b) respectively. For $\epsilon = 0$ we observe no change in N_{eff} with g_X in Fig.9(a) as argued in the previous sections in the context of Fig.7(a). On the other hand, for $\epsilon = -g_X/70$ we observe the non-trivial dependence of N_{eff} with g_X in Fig.9(a) due to the interplay between scattering and decays as elaborated in detail in the context of Fig.7(b).

In the same plane for both the plots Fig.9(a) and Fig.9(b) we portray the constraints arising from $E\nu\text{ES}$ experiment with XENON1T[20] shown by the regions shaded by dark cyan diagonal lines. Similarly, we showcase the exclusion region from Borexino depicted by magenta shaded region. Note that these bounds are weaker for $U(1)_{B_3-3L_\mu}$ compared to Fig.8 as in this case Z' has no tree level coupling with e^\pm and the recoil rate gets smaller here (see eq.(10)). Because, in this scenario Z' couples directly with μ , the Neutrino trident experiment significantly constrains the parameter space shown by the dark blue dashed dot line [22]. The parameter space above that line is excluded. In this model also Z' can generate $B_s - \bar{B}_s$ mixing and attracts constraint depicted by orange shaded region [22]. Similar to the previous subsection the bound from $\text{CE}\nu\text{NS}$ experiment is weaker than $E\nu\text{ES}$ and hence not shown in Fig.9. The bound from supernova cooling is shown by the region shaded with grey vertical lines [6]. We do not show the results for $U(1)_{B_3-3L_\tau}$ explicitly, though the imprint in N_{eff} for this model will be similar like the one in $U(1)_{B_3-3L_\tau}$ as both these models have

$$|X_1| = 0.$$

6. THE NEUTRINO PORTAL SOLUTION TO THE HUBBLE TENSION

The change in N_{eff} due to the presence of light Z' gauge bosons can also lead to an interesting consequence namely a simple and elegant resolution to the cosmological Hubble constant problem. Recall that the Hubble constant problem is the discrepancy between the obtained value of the Hubble constant using early and late time probes [30, 33]. As mentioned in the introduction the discrepancy in H_0 value can be ameliorated with increasing N_{eff} [30]. Several different resolutions have been proposed to address this discrepancy. One of the simplest possible resolution is the presence of light degrees of freedom changing the N_{eff} [6, 9, 17, 18]. There are already a few model specific works successfully addressing this problem for particular $U(1)_X$ extensions such as $U(1)_{\mu-\tau}$ [6] and $U(1)_{B-L}$ [46].

The general formalism developed in this work also can be used to show that the $U(1)_X$ symmetries with light Z' gauge bosons, in general, can address the Hubble constant problem reducing the tension. According to the Planck 2015 TT data [30, 37], the H_0 tension issue can be relaxed upto 1.8σ with the N_{eff} value between 3.2 to 3.5. However, the Planck 2018 polarization measurements provide a more stringent bound on N_{eff} [4] and it is difficult to reach $H_0 > 70 \text{ Km s}^{-1}\text{Mpc}^{-1}$ [67] within the ΛCDM . Hence there still exists a disagreement of 3.6σ in the H_0 value predicted from CMB and local measurement. In our discussion, we only highlight the parameter space where N_{eff} lies between 3.2 to 3.5 in $M_{Z'} - g_X$ plane, that may relax H_0 tension followed by the analysis in ref. [30, 37]. In sec.4 we portray the parameter space for generic $U(1)_X$ models in Fig.6 (for $|X_1| \neq 0$) and Fig.7 ($|X_1| = 0$) where the blue and red dashed lines indicate the values of $N_{\text{eff}} = 3.2$ and 3.5 respectively. Similarly, in sec.5 we also showcase the same lines with constant $N_{\text{eff}} = 3.2$ (blue dashed line) and 3.5 (red dashed line) contours for the specific models: $U_{B_3-3L_e}$ (in Fig.8) and $U_{B_3-3L_\mu}$ (in Fig. 9). The region between these two contour lines may ameliorate H_0 tension. However claiming any possible resolution of H_0 problem with quantitative effectiveness, itself requires a dedicated analysis which is beyond the scope of this work [30].

7. SUMMARY AND CONCLUSION

The Planck experiment has a very accurate measurement of the CMB which has established stringent limits on ΔN_{eff} , representing the number of effective relativistic degrees of freedom during the early epoch of the universe [4]. This sensitivity makes ΔN_{eff} a useful probe for investigating various BSM scenarios that affect the neutrino decoupling at the time of the CMB. In this work, we have studied the impact of light Z' particle, arising from generic $U(1)_X$ model, on N_{eff} . In the presence of this light Z' , N_{eff} receives two-fold contributions: the decay of $Z' \rightarrow \nu_L \bar{\nu}_L$, $e^+ e^-$ and scattering of light SM leptons (ν_L, e) via

this Z' . At first, we considered a generic $U(1)_X$ model with arbitrary charge assignments. Apart from the light Z' gauge boson, the model also contains a BSM scalar σ and RHN ν_R which are necessary for the model construction. To understand the sole effect of the light Z' in early universe temperature evolution, we assume the other BSM particles are sufficiently heavy ($\gtrsim 100$ MeV) that they decouple at the time of neutrino decoupling. In this work, we only consider the scenario where Z' was initially ($T \gtrsim M_{Z'}$) in a thermal bath and leave the other scenario with non-thermal Z' for future work [56]. We adopt the formalism developed in ref.[6] and solve the temperature equations to evaluate N_{eff} in sec.3. We enumerate our findings below.

- Firstly, we noticed that the $U(1)_X$ charges for $e, \nu_{e,\mu,\tau}$ play a crucial role in N_{eff} for our proposed generic $U(1)_X$ model in sec.2 as these are the only SM particles relevant for ν decoupling. In a similar vein, we found that the mass of the BSM gauge boson Z' should be around $\lesssim 30$ MeV to affect neutrino decoupling.
- After a careful analysis in sec.3 we observed that the value of N_{eff} depends differently on the coupling g_X for two distinct scenarios those are $|X_1| = 0$ and $|X_1| \neq 0$. Based on this fact, in sec.4 we categorise $U(1)_X$ models into two classes: (a) electrons having tree level coupling with Z' ($|X_1| = 0$) and (b) without tree level coupling of an electron with Z' ($|X_1| \neq 0$). However, in the second scenario electron may have some induced coupling with Z' even if $|X_1| = 0$ and we explored that scenario too. For both the two classes we present the contours from the upper limit on N_{eff} from Planck 2018 [4] in $M_{Z'}$ vs. g_X plane as shown in Fig.6 and Fig.7. In the same plane, we also highlight the parameter space favoured to relax H_0 tension shown in earlier analyses [6, 37].
- As an example model, in sec.5 we considered a specific $U(1)_X$ model and discuss the cosmological implications in context of N_{eff} . We present the numerical results for $U(1)_{B_3-3L_e}$ ($|X_1| = 3$) and $U(1)_{B_3-3L_\mu}$ ($|X_1| = 0$) models in sub-sec.5.1 and sub-sec.5.2 respectively. Depending on the coupling of an electron with Z' these two models also lead to distinguishable N_{eff} contours in $M_{Z'}$ vs. g_X plane as portrayed in Fig.8 and Fig.9.
- For both $U(1)_{B_3-3L_e}$ and $U(1)_{B_3-3L_\mu}$ models we also showcase the relevant astrophysical and laboratory constraints in Fig.8 and Fig.9 respectively. We displayed the constraints from $\text{E}\nu\text{ES}$ with XENON1T [20] and Borexino [58], neutrino trident [22], $B_s - \overline{B}_s$ mixing [22] as well as from SN1987A [6]. We checked the constraints from $\text{CE}\nu\text{NS}$ [20] is weaker than the other constraints as our chosen $U(1)_X$ models do not have Z' coupling with first generation quarks. For $U(1)_{B_3-3L_\mu}$ model electron has no BSM gauge coupling and hence, the bounds from $\text{E}\nu\text{ES}$ for this model are weaker than the other one. In the same plane, we also indicate the parameter space that can relax the H_0 tension [6, 37].

For both $U(1)_{B_3-3L_e}$ and $U(1)_{B_3-3L_\mu}$ models we have shown that the bounds on N_{eff} from Planck 2018 data [4] can provide more stringent bound on the parameter space than the laboratory searches. The future generation experiments like CMB-S4 ($\Delta N_{\text{eff}} = 0.06$ at 2σ) [68] can even probe more parameter space for such models. Our analysis also shows that there is a certain parameter space still left to relax H_0 tension [6, 37] allowed from all kinds of constraints. On the other hand, as $U(1)_X$ models are well motivated BSM scenarios and widely studied in several aspects, this analysis may enhance insights to explore their connection with the H_0 problem too. Our generalised prescription for N_{eff} analysis with generic $U(1)_X$ models is extremely helpful to put stringent constraints on the parameter space from cosmology complementary to the bounds obtained from ground based experiments. In this analysis we considered the thermal Z' scenario only and hence the bounds from N_{eff} for extremely small couplings are not shown. However, in future, we will explore the non-thermal Z' scenario also to constrain the parameter space from N_{eff} even for the smaller Z' mass and couplings [56].

Acknowledgments

SJ thanks Sougata Ganguly for the helpful discussion and Miguel Escudero for the email conversations. The work of SJ is funded by CSIR, Government of India, under the NET JRF fellowship scheme with Award file No. 09/080(1172)/2020-EMR-I. PG would like to acknowledge the Indian Association for the Cultivation of Science, Kolkata for the financial support.

Appendix A: Neutrino decoupling in SM scenario

In this section, we recapitulate the formalism for ν_L decoupling in the SM scenario which is already developed in ref.[5]. However, for better understanding and smooth transition to the extra $U(1)_X$ scenario we just note down the key points for the SM case here. As mentioned in sec.3 the only particles relevant at the temperature scale of ν_L decoupling are ν_i ($i = e, \mu, \tau$), e^\pm and γ . So in the SM scenario, the temperature evaluation of only these 3 particles is needed to evaluate T_ν/T_γ . Initially all ν_i ($i = e, \mu, \tau$) were coupled to γ and e^\pm bath at high temperature via weak interaction processes. To track the exact temperature of photon bath (T_γ) and neutrino bath (T_ν) we start from the Liouville equation [50]:

$$\frac{\partial f(p, t)}{\partial t} - H f(p, t) \frac{\partial f(p, t)}{\partial p} = \mathcal{C}[f], \quad (\text{A1})$$

where, $f(p, t)$ is the distribution function in a homogeneous and isotropic universe and p, t signifies the momentum and time respectively. $\mathcal{C}[f]$ is the collision term and it describes the total change in $f(p, t)$ with time.

For SM ν_L decoupling the involved processes are $2 \rightarrow 2$ scattering between ν, e as shown in Table IV. So, we write the collision terms for a particle χ undergoing $2 \rightarrow 2$ process say, $\chi + i \rightarrow j + k$ for which $\mathcal{C}[f]$ can be written as (assuming CP invariance),

$$\mathcal{C}[f_\chi] \equiv -\frac{1}{2E_\chi} \int d\Pi_i d\Pi_j d\Pi_k (2\pi)^4 \delta^4(p_\chi + p_i - p_j - p_k) \times |\mathcal{M}|_{\chi+i \rightarrow j+k}^2 [f_\chi f_i [1 \pm f_j] [1 \pm f_k] - f_j f_k [1 \pm f_\chi] [1 \pm f_i]] \quad (\text{A2})$$

where, f_ℓ, E_ℓ , and p_ℓ denote the distribution function, energy, and 4-momentum respectively for particle ℓ . $|\mathcal{M}|_{\chi+i \rightarrow j+k}^2$ is the amplitude square for the above mentioned process.

Multiplying eq.(A1) with $g_\chi E d^3p_\chi / (2\pi)^3$ and integrating over momenta will give the following energy density equation:

$$\frac{d\rho_\chi}{dt} + 3H(\rho_\chi + P_\chi) = \int g_\chi E \frac{d^3p_\chi}{(2\pi)^3} \mathcal{C}[f_\chi] = \frac{\delta\rho_{\chi \rightarrow j}}{\delta t} \quad (\text{A3})$$

$\frac{\delta\rho_{\chi \rightarrow j}}{\delta t}$ is the energy density transfer rate from $\chi \rightarrow j$ (or k). P_χ is the pressure density. So, we can rewrite energy density equation eq.(A3) for χ ,

$$\frac{dT_\chi}{dt} = \left(-3H(\rho_\chi + P_\chi) + \frac{\delta\rho_\chi}{\delta t} \right) \left(\frac{\partial\rho_\chi}{\partial T_\chi} \right)^{-1} \quad (\text{A4})$$

Now for SM ν_L decoupling we consider the energy transfers between ν_i ($i = e, \mu, \tau$) to e^\pm, γ photon bath. For photon bath containing γ, e^\pm we consider a common temperature T_γ and add their energy density equations and rearrange accordingly,

$$\frac{d\rho_\gamma}{dt} + \frac{d\rho_e}{dt} = -4H\rho_\gamma - 3H(\rho_e + P_e) + \sum_{i=e,\mu,\tau} \frac{\delta\rho_{e \rightarrow \nu_i}}{\delta t} \quad (\text{A5})$$

$$\frac{dT_\gamma}{dt} = \left(-4H\rho_\gamma - 3H(\rho_e + P_e) - \sum_{i=e,\mu,\tau} \frac{\delta\rho_{\nu_i \rightarrow e}}{\delta t} \right) \left(\frac{\partial\rho_\gamma}{\partial T_\gamma} + \frac{\partial\rho_e}{\partial T_\gamma} \right)^{-1}, \quad (\text{A6})$$

where, in the last step we have used $\frac{\delta\rho_{\nu_\chi \rightarrow j}}{\delta t} = -\frac{\delta\rho_{j \rightarrow \chi}}{\delta t}$. Similarly, following eq.(A3) we can write the respective temperature (T_{ν_i}) equations for each type of ν ,

$$\frac{dT_{\nu_i}}{dt} = \left(-4H\rho_{\nu_i} + \frac{\delta\rho_{\nu_i}}{\delta t} \right) \left(\frac{\partial\rho_{\nu_i}}{\partial T_{\nu_i}} \right)^{-1} \quad (\text{A7})$$

Once we have the temperature equations the remaining step is to evaluate the energy transfer rates i.e. the collision terms. The relevant processes in the SM scenario are given in Table IV.

All the processes are either elastic scatterings between ν_i and e or annihilations and all are mediated by W^\pm, Z . As we are focusing on the MeV scale we can integrate out the mediators and write in terms of Fermi constant G_F . In Table IV, $p_{1,2}$ and $p_{3,4}$ denote the momentum

Process	$2^{-5}G_F^2 M ^2$
$\nu_i + \bar{\nu}_i \longleftrightarrow e^+ + e^-$	$4[g_{L_i}^2(p_1 \cdot p_4)(p_2 \cdot p_3) + g_{R_i}^2(p_1 \cdot p_3)(p_2 \cdot p_4)]$
$\nu_i + e^- \longleftrightarrow \nu_i + e^-$	$4[g_{L_i}^2(p_1 \cdot p_2)(p_3 \cdot p_4) + g_{R_i}^2(p_1 \cdot p_4)(p_2 \cdot p_3)]$
$\nu_i + e^+ \longleftrightarrow \nu_i + e^+$	$4[g_{L_i}^2(p_1 \cdot p_4)(p_2 \cdot p_3) + g_{R_i}^2(p_1 \cdot p_2)(p_3 \cdot p_4)]$
$\nu_i + \nu_j \longleftrightarrow \nu_i + \nu_j$	$(p_1 \cdot p_2)(p_3 \cdot p_4)$
$\nu_i + \bar{\nu}_j \longleftrightarrow \nu_i + \bar{\nu}_j$	$(p_1 \cdot p_2)(p_3 \cdot p_4)$

TABLE IV: Squared amplitudes for interactions relevant for ν decoupling in SM. The i in subscripts stand for different generations of ν_L [52].

of incoming and outgoing particles. Here, $g_{L_e} = \frac{1}{2} + s_W^2$, $g_{R_e} = s_W^2$, $g_{L_{\mu,\tau}} = -\frac{1}{2} + s_W^2$, $g_{R_{\mu,\tau}} = s_W^2$ and $s_W = \sin \theta_W$ where θ_W is Weinberg angle. The reason behind the difference of 1 between g_{L_e} and $g_{R_{\mu,\tau}}$ is the additional charged current process available for ν_e .

Collision terms for ν, e^\pm scattering

Process	$\pi^5 G_F^{-2} \frac{\delta \rho}{\delta t}$
$\nu_i + \bar{\nu}_i \longleftrightarrow e^+ + e^-$	$64(g_{L_i}^2 + g_{R_i}^2) [T_\gamma^9 - T_{\nu_i}^9]$
$\nu_i + e^\pm \longleftrightarrow \nu_i + e^\pm$	$112(g_{L_i}^2 + g_{R_i}^2) T_\gamma^4 T_{\nu_i}^4 [T_\gamma - T_{\nu_i}]$
$\nu_i + \bar{\nu}_i \longleftrightarrow \nu_j + \bar{\nu}_j$	$32 [T_{\nu_j}^9 - T_{\nu_i}^9]$
$\nu_i + \nu_j \longleftrightarrow \nu_i + \nu_j$	$48 T_{\nu_j}^4 T_{\nu_i}^4 [T_{\nu_j} - T_{\nu_i}]$
$\nu_i + \bar{\nu}_j \longleftrightarrow \nu_i + \bar{\nu}_j$	$8 T_{\nu_j}^4 T_{\nu_i}^4 [T_{\nu_j} - T_{\nu_i}]$

TABLE V: Collision terms for ν, e^\pm scattering assuming MB distribution function [5, 47]. The i in subscripts stand for different generations of ν_L .

The first 2 processes are responsible for energy transfer from ν_e to e sector (photon bath) and the rest are responsible for energy transfer from ν_e to $\nu_{\mu/\tau}$ sector. Finally, we enumerate below all the energy transfer rates for the SM scenario following the formalism in ref.[5, 47]:

$$\left(\frac{\delta \rho_{\nu_e \rightarrow e}}{\delta t} \right)_{\text{SM}} = \frac{G_F^2}{\pi^5} \{ (1 + 4s_W^2 + 8s_W^4) F_{\text{MB}}(T_\gamma, T_{\nu_e}) \} \quad (\text{A8})$$

$$\left(\frac{\delta \rho_{\nu_{\mu/\tau} \rightarrow e}}{\delta t} \right)_{\text{SM}} = \frac{G_F^2}{\pi^5} \{ (1 - 4s_W^2 + 8s_W^4) F_{\text{MB}}(T_\gamma, T_{\nu_\mu}) \} \quad (\text{A9})$$

$$\left(\frac{\delta \rho_{\nu_e \rightarrow \mu/\tau}}{\delta t} \right)_{\text{SM}} = \frac{G_F^2}{\pi^5} F_{\text{MB}}(T_{\nu_\mu}, T_{\nu_e}), \quad (\text{A10})$$

where,

$$F_{\text{MB}}(T_1, T_2) = 32 (T_1^9 - T_2^9) + 56 T_1^4 T_2^4 (T_1 - T_2). \quad (\text{A11})$$

Plugging these collision terms in eq.(A6) and eq.(A7) we can track the temperature evolution.

Appendix B: Neutrino decoupling in presence of a $U(1)_X$ gauge boson

The relevant lagrangian for the calculation of N_{eff} in $U(1)_X$ model has the following generic form,

$$\mathcal{L}_{\text{int}} \supset Z'_\alpha J_{\mathbb{X}}^\alpha, \quad (\text{B1})$$

where, $J_{\mathbb{X}}^\alpha$ is the Noether current associated with $U(1)_{\mathbb{X}}$ and given by,

$$\begin{aligned} J_{\mathbb{X}}^\alpha = & g_X (X_3 \bar{\tau} \gamma^\alpha \tau + X_3 \bar{\nu}_\tau \gamma^\alpha P_L \nu_\tau + X_2 \bar{\mu} \gamma^\alpha \mu + X_2 \bar{\nu}_\mu \gamma^\alpha P_L \nu_\mu) \\ & + g_X (X_1 \bar{e} \gamma^\alpha e + X_1 \bar{\nu}_e \gamma^\alpha P_L \nu_e) \end{aligned} \quad (\text{B2})$$

We have not written the corresponding interactions with quark sectors since around ~ 2 MeV quarks are already confined [69]. The μ, τ particles also do not take part as they have suppressed energy density around MeV temperature. In the presence of these Z' the following things will affect neutrino decoupling (see Fig.1).

1. Depending on charge assignments ($X_1 \neq 0$) Z' can decay to e^+e^- and the inverse decay can also happen upto $T_\gamma = M_{Z'}$. So there will be energy transfer from Z' to e^\pm sector(γ bath) and vice versa. Similarly, Z' can transfer energy to ν bath with the decays and inverse decays to $\nu_i \bar{\nu}_i$.
2. Through Z' portal $\nu_i + \bar{\nu}_i \longleftrightarrow e^+e^-$, $\nu_i + e^\pm \longleftrightarrow \nu_i + e^\pm$, $i = (e, \mu, \tau)$ processes can happen (depending on $X_{1,2,3}$) leading to an additional energy transfer between ν_i sector and e^\pm .

We will discuss the above points in the following subsections. As discussed in Sec.3, in this work we will only focus on the scenarios where Z' was in thermal equilibrium with e, ν_i at $T > T_{\text{dec}}^\nu$.

1. Z' decay to e^+e^-

We consider the process

$$Z'(k) \leftrightarrow e^-(p_1) + e^+(p_2), \quad (\text{B3})$$

where, k, p_1, p_2 denote the four momenta of respective particles. Following eq.(A2) and eq.(A3) we calculate the energy transfer rate from Z' to e bath,

$$\int g_{Z'} E_{Z'} \frac{d^3 k}{(2\pi)^3 2E_{Z'}} \mathcal{C}[f] = - \int g_{Z'} \frac{d^3 k}{(2\pi)^3 2E_{Z'}} g_1 \frac{d^3 p_1}{(2\pi)^3 2E_1} g_2 \frac{d^3 p_2}{(2\pi)^3 2E_2} E_{Z'} \frac{1}{g_{Z'} g_1 g_2} |\mathcal{M}_{e^+e^- \rightarrow Z'}|^2 (f_{z'}^{(\text{eq})}(k) - f_e^{(\text{eq})}(p_1) f_e^{(\text{eq})}(p_2)) (2\pi)^4 \delta^4(p_1 + p_2 - k) \quad (\text{B4})$$

Here the degrees of freedom and energy of the corresponding particle are denoted as $g_\ell \& E_\ell$, ($\ell \equiv Z', 1, 2$) respectively. f_i^{eq} , ($i \equiv Z', e$) signify the equilibrium distribution function of i particle

The decay width of Z' to e^+e^- is given by,

$$\Gamma_{Z' \rightarrow e^+e^-} = \frac{1}{2M_{Z'}} \int \frac{d^3 p_1}{(2\pi)^3 2E_1} \frac{d^3 p_2}{(2\pi)^3 2E_2} \frac{1}{g_{Z'}} |\mathcal{M}_{Z' \rightarrow e^+e^-}|^2 (2\pi)^4 \delta^4(p_1 + p_2 - p_k) \quad (\text{B5})$$

$$= X_1^2 \frac{g_X^2 M_{Z'}}{12\pi} \left(1 + \frac{2m_e^2}{M_{Z'}^2}\right) \sqrt{1 - \frac{4m_e^2}{M_{Z'}^2}} \quad (\text{B6})$$

where m_e is the electron mass.

Using eq.(B6) we can simplify above eq.(B4) as

$$\int g_{z'} E_k \frac{d^3 k}{(2\pi)^3 2E_k} \mathcal{C}[f] = \frac{3M_{Z'}^3 \Gamma_{Z' \rightarrow e^+e^-}}{2\pi^2} \left[T_\gamma K_2 \left(\frac{M_{Z'}}{T_\gamma} \right) - T_{Z'} K_2 \left(\frac{M_{Z'}}{T_{Z'}} \right) \right] \quad (\text{B7})$$

Therefore, from eq.(A2) we write

$$\frac{\delta \rho_{Z' \rightarrow e}}{\delta t} = \frac{3m_{Z'}^3}{2\pi^2} \left[T_\gamma K_2 \left(\frac{M_{Z'}}{T_\gamma} \right) - T_{Z'} K_2 \left(\frac{M_{Z'}}{T_{Z'}} \right) \right] \Gamma_{Z' \rightarrow e^+e^-}, \quad (\text{B8})$$

$T_{Z'}$ denotes temperature of Z' bath.

2. Z' decay to $\nu_i \bar{\nu}_i$

Here we consider the processes

$$Z'(k) \leftrightarrow \nu_i(p_1) + \bar{\nu}_i(p_2), \quad \text{where } i = e, \mu, \tau. \quad (\text{B9})$$

The corresponding decay widths of Z' to i type ν are given as,

$$\Gamma_{Z' \rightarrow \nu_i \bar{\nu}_i} = X_i^2 \frac{g_X^2 M_{Z'}}{24\pi}. \quad (\text{B10})$$

Similar to the previous section we can write the energy density transfer rates from Z' to each generation of ν as,

$$\frac{\delta\rho_{Z'\rightarrow\nu_i}}{\delta t} = \frac{3m_{Z'}^3}{2\pi^2} \left[T_{\nu_i} K_2 \left(\frac{M_{Z'}}{T_{\nu_i}} \right) - T_{Z'} K_2 \left(\frac{M_{Z'}}{T_{Z'}} \right) \right] \Gamma_{Z'\rightarrow\nu_i\bar{\nu}_i}, \quad (\text{B11})$$

3. Energy transfer from ν_i to e^+e^- mediated by BSM Z'

In the presence of light Z' there will be additional energy transfer between e^\pm and ν_i apart from the SM weak processes (mediated by SM $W\&Z$). The two relevant processes are:

$$\nu(p_1) + \bar{\nu}(p_2) \leftrightarrow e^-(p_3) + e^+(p_4) \quad (\text{B12})$$

$$\nu(p_1) + e^\pm(p_2) \leftrightarrow \nu(p_3) + e^\pm(p_4) \quad (\text{B13})$$

We denote the amplitudes for SM and BSM processes as \mathcal{M}_{SM} and \mathcal{M}_{BSM} respectively. Then the total amplitude \mathcal{M}_{tot} can be written as

$$|\mathcal{M}_{\text{tot}}|^2 = |\mathcal{M}_{\text{SM}}|^2 + 2\text{Re}(\mathcal{M}_{\text{SM}}\mathcal{M}_{\text{BSM}}^\dagger) + |\mathcal{M}_{\text{BSM}}|^2 \quad (\text{B14})$$

Plugging this in eq.(A2) we will get the total energy transfer rate ($\nu \leftrightarrow e$) Three sources contribute to the total energy transfer rate; pure SM, SM-BSM interference, and pure BSM respectively. For simplicity, we calculate the energy transfer rates for each of them separately. The amplitudes for pure SM contributions can be found in sec.A. And the energy transfer rates for pure SM contributions are given in eq.(A8- A10) [5].

The amplitude for BSM processes (with proper momentum assignment) will be ($s \ll M_{Z'}^2$)

$$\mathcal{M}_{\text{BSM}} = -\frac{(X_i g_X)(X_1 g_X)}{M_{Z'}^2} [\bar{\nu}_i \gamma^\mu P_L \nu_i] [\bar{e} \gamma_\mu e] \quad (\text{B15})$$

The interference amplitudes in eq.(B14) are tabulated in Tab.-VI.

Process	$2^{-3}/\sqrt{2} G_F (X_i g_X)^{-1} (X_1 g_X)^{-1} M_{Z'}^2 M ^2$
$\nu_i + e^- \longleftrightarrow \nu_i + e^-$	$1/2 [g_L(p_1 \cdot p_2)(p_3 \cdot p_4) + g_R(p_1 \cdot p_4)(p_2 \cdot p_3)]$
$\nu_i + e^+ \longleftrightarrow \nu_i + e^+$	$1/2 [g_L(p_1 \cdot p_4)(p_2 \cdot p_3) + g_R(p_1 \cdot p_2)(p_3 \cdot p_4)]$
$\nu_i + \bar{\nu}_i \longleftrightarrow e^+ + e^-$	$[g_L(p_1 \cdot p_4)(p_2 \cdot p_3) + g_R(p_1 \cdot p_3)(p_2 \cdot p_4)]$

TABLE VI: Relevant SM-BSM interference terms for ν decoupling in SM. The interactions are written with i ($i = e, \mu, \tau$) type ν .

Following the formalism developed in ref.[47] we write the collision terms for the inter-

ference terms:

$$\int \frac{d^3p}{2\pi^3} p \mathcal{C}[f]_{\nu_i+e\leftrightarrow\nu_i+e} = (X_i g_X)(X_1 g_X) \frac{7\sqrt{2}G_F}{\pi^5 M_{Z'}^2} (g_L + g_R) T_\gamma^4 T_{\nu_i}^4 [T_\gamma - T_{\nu_i}] \quad (\text{B16})$$

$$\int \frac{d^3p}{2\pi^3} p \mathcal{C}[f]_{\nu_i\bar{\nu}_i\leftrightarrow ee} = (X_i g_X)(X_1 g_X) \frac{4\sqrt{2}G_F}{\pi^5 M_{Z'}^2} (g_L + g_R) [T_\gamma^9 - T_{\nu_i}^9] \quad (\text{B17})$$

The first one in the above two collision terms accounts for elastic scattering of ν_i with both e^\pm . Here we have multiplied with an additional factor 2 to count the effect of $\bar{\nu}_i$. The second collision term in eq.(B17) is due to annihilations. So, the total energy transfer rate from ν to e bath due to the interference with $U(1)_X$ gauge boson,

$$\left(\frac{\delta\rho_{\nu_i\rightarrow e}}{\delta t} \right)_{\text{int}} = (X_i g_X)(X_1 g_X) \frac{\sqrt{2}G_F}{8\pi^5 M_{Z'}^2} \{(g_L + g_R)F_{\text{MB}}(T_\gamma, T_{\nu_i})\}, \quad (\text{B18})$$

In a similar fashion, we now move to calculate the collision term due to pure BSM amplitudes (third term in eq.(B14)). The pure BSM amplitudes in eq.(B14) are tabulated in Tab.-VII.

Process	$2^{-4} (X_i g_X)^{-2} (X_1 g_X)^{-2} M_{Z'}^2 \overline{ M ^2}$
$\nu_i + e^- \longleftrightarrow \nu_i + e^-$	$1/2 [(p_1 \cdot p_2)(p_3 \cdot p_4) + (p_1 \cdot p_4)(p_2 \cdot p_3)]$
$\nu_i + e^+ \longleftrightarrow \nu_i + e^+$	$1/2 [(p_1 \cdot p_4)(p_2 \cdot p_3) + (p_1 \cdot p_2)(p_3 \cdot p_4)]$
$\nu_i + \bar{\nu}_i \longleftrightarrow e^+ + e^-$	$[(p_1 \cdot p_4)(p_2 \cdot p_3) + (p_1 \cdot p_3)(p_2 \cdot p_4)]$

TABLE VII: Relevant BSM terms for ν decoupling in the SM. The interactions are written with i ($i = e, \mu, \tau$) type ν .

The collision terms will be:

$$\int \frac{d^3p}{2\pi^3} p \mathcal{C}[f]_{\nu_i+e\leftrightarrow\nu_i+e} = (X_i g_X)^2 (X_1 g_X)^2 \frac{14}{\pi^5 M_{Z'}^4} T_\gamma^4 T_{\nu_i}^4 [T_\gamma - T_{\nu_i}] \quad (\text{B19})$$

$$\int \frac{d^3p}{2\pi^3} p \mathcal{C}[f]_{\nu_i\bar{\nu}_i\leftrightarrow ee} = (X_i g_X)^2 (X_1 g_X)^2 \frac{8}{\pi^5 M_{Z'}^4} [T_\gamma^9 - T_{\nu_i}^9] \quad (\text{B20})$$

So, the total energy transfer rate from ν to e bath due to the pure BSM matrix element of $U(1)_X$ gauge boson,

$$\left(\frac{\delta\rho_{\nu_i\rightarrow e}}{\delta t} \right)_{\text{BSM}} = (X_i g_X)^2 (X_1 g_X)^2 \frac{1}{4\pi^5 M_{Z'}^4} F_{\text{MB}}(T_\gamma, T_{\nu_i}), \quad (\text{B21})$$

So the total energy transfer rate from ν_i to e bath will be

$$\left(\frac{\delta\rho_{\nu_i\rightarrow e}}{\delta t}\right)_{\text{tot}} = \left(\frac{\delta\rho_{\nu_i\rightarrow e}}{\delta t}\right)_{\text{SM}} + \left(\frac{\delta\rho_{\nu_i\rightarrow e}}{\delta t}\right)_{\text{int}} + \left(\frac{\delta\rho_{\nu_i\rightarrow e}}{\delta t}\right)_{\text{BSM}} \quad (\text{B22})$$

$X_1 = 0$: Here we would like to highlight the scenarios where $X_1 = 0$. In such case apparently, it seems that the BSM contributions in eq.(B4),eq.(B20),eq.(B21) vanish. However, in such cases even though Z' doesn't have any tree level coupling with e^\pm , it can couple to e^\pm through induced couplings which may generate from kinetic mixing, fermion loops or CKM mixing. If the loop factor induced coupling is denoted as ϵ , then in such cases we have to just replace the term $(X_1 g_X)$ in eq.(B4),eq.(B20),eq.(B21) with ϵe .

$$(X_1 g_X) \longrightarrow (\epsilon e) \quad (\text{for } X_1 = 0) \quad (\text{B23})$$

So, even if $X_1 = 0$, there can be energy transfer from Z' to e bath as well as ν_i to e bath by Z' mediation.

Note that eq.(B22) differs from ref.[6] where the authors ignored the SM-BSM interference term in the calculation of energy transfer rates. However, our BSM contribution term $\left(\frac{\delta\rho_{\nu_i\rightarrow e}}{\delta t}\right)_{\text{BSM}}$ in eq.(B21) agrees with ref.[6] for a specific choice of $U(1)_X$ ($U(1)_{L_\mu-L_\tau}$).

4. Temperature evolution

Now with all the collision terms, we are set to formulate the energy evaluation equations. Following the prescription in appendix-A we can write the following energy density evaluation equations:

$$\frac{d\rho_{\nu_i}}{dt} = - \left(4H\rho_{\nu_i} - \left(\frac{\delta\rho_{\nu_i\rightarrow e}}{\delta t}\right)_{\text{tot}} - \sum_{j\neq i} \left(\frac{\delta\rho_{\nu_i\rightarrow\nu_j}}{\delta t}\right)_{\text{tot}} + \frac{\delta\rho_{Z'\rightarrow\nu_i}}{\delta t} \right) \quad (\text{B24})$$

$$\frac{d\rho_{Z'}}{dt} = - \left(3H(\rho_{Z'} + P_{Z'}) - \sum_i \frac{\delta\rho_{Z'\rightarrow\nu_i}}{\delta t} - \frac{\delta\rho_{Z'\rightarrow e}}{\delta t} \right) \quad (\text{B25})$$

$$\frac{d\rho_\gamma}{dt} = - \left(4H\rho_\gamma + 3H(\rho_e + p_e) + \sum_i \left(\frac{\delta\rho_{\nu_i\rightarrow e}}{\delta t}\right)_{\text{tot}} + \frac{\delta\rho_{Z'\rightarrow e}}{\delta t} \right), \quad (\text{B26})$$

where the \sum_i indicates the summation of energy density transfer rates over all 3 generation of ν (e, μ, τ). And $\left(\frac{\delta\rho_{\nu_i\rightarrow\nu_j}}{\delta t}\right)_{\text{tot}}$ bears a similar kind of form as in the SM case. However, in the presence of the light Z' , it will get some additional contribution from Z' mediation. So the G_F^2 in eq.(A10) will be simply replaced by $G_F \rightarrow (G_F + (X_i g_X)(X_j g_X)/M_{Z'}^2)$. Similar to the previous section we can write the temperature evaluation equations using the partial

derivatives and we get,

$$\frac{dT_{\nu_i}}{dt} = - \left(4H\rho_{\nu_i} - \left(\frac{\delta\rho_{\nu_i \rightarrow e}}{\delta t} \right)_{\text{tot}} - \sum_{j \neq i} \left(\frac{\delta\rho_{\nu_i \rightarrow \nu_j}}{\delta t} \right)_{\text{tot}} + \frac{\delta\rho_{Z' \rightarrow \nu_i}}{\delta t} \right) \left(\frac{\partial\rho_{\nu_i}}{\partial T_{\nu_i}} \right)^{-1} \quad (\text{B27})$$

$$\frac{dT_{Z'}}{dt} = - \left(3H(\rho_{Z'} + P_{Z'}) - \sum_i \frac{\delta\rho_{Z' \rightarrow \nu_i}}{\delta t} - \frac{\delta\rho_{Z' \rightarrow e}}{\delta t} \right) \left(\frac{\partial\rho_{Z'}}{\partial T_{Z'}} \right)^{-1} \quad (\text{B28})$$

$$\frac{dT_{\gamma}}{dt} = - \left(4H\rho_{\gamma} + 3H(\rho_e + p_e) + \sum_i \left(\frac{\delta\rho_{\nu_i \rightarrow e}}{\delta t} \right)_{\text{tot}} + \frac{\delta\rho_{Z' \rightarrow e}}{\delta t} \right) \left(\frac{\partial\rho_{\gamma}}{\partial T_{\gamma}} + \frac{\partial\rho_e}{\partial T_{\gamma}} \right)^{-1} \quad (\text{B29})$$

Hence solving the aforementioned five Boltzmann equations one can track the evolution of ν_L decoupling. By exploiting the neutrino oscillations which are active around $\sim \text{MeV}$ temperature [41, 51–53], one can further simplify the scenario by assuming all 3 ν_i equilibrate with each other and acquire a common temperature i.e. $T_{\nu_e} = T_{\nu_{\mu}} = T_{\nu_{\tau}} \equiv T_{\nu}$. The benefit of such an assumption is that we no longer have to keep track of the energy transfer rates within different ν sectors i.e. $\left(\frac{\delta\rho_{\nu_i \rightarrow \nu_j}}{\delta t} \right)_{\text{tot}} = 0$ in eq.(B27). In such case the three T_{ν_i} equations (eq.(B27)) simply reduce to a single temperature (T_{ν}) evaluation equation:

$$\frac{dT_{\nu}}{dt} = - \left(4H\rho_{\nu} - \left(\frac{\delta\rho_{\nu \rightarrow e}}{\delta t} \right)_{\text{tot}} + \frac{\delta\rho_{Z' \rightarrow \nu}}{\delta t} \right) \left(\frac{\partial\rho_{\nu}}{\partial T_{\nu}} \right)^{-1}, \quad (\text{B30})$$

where, $\rho_{\nu} = \sum_{i=e,\mu,\tau} \rho_{\nu_i}$, $\left(\frac{\delta\rho_{\nu \rightarrow e}}{\delta t} \right)_{\text{tot}} = \sum_{i=e,\mu,\tau} \left(\frac{\delta\rho_{\nu_i \rightarrow e}}{\delta t} \right)_{\text{tot}}$ and $\frac{\delta\rho_{Z' \rightarrow \nu}}{\delta t} = \sum_{i=e,\mu,\tau} \frac{\delta\rho_{Z' \rightarrow \nu_i}}{\delta t}$

Appendix C: Evaluation of N_{eff} with different T_{ν_i}

Throughout the paper we evaluated N_{eff} assuming all three ν_i , ($i \equiv e, \mu, \tau$) share the same temperature. However, the values of N_{eff} change if we allow all ν_i to develop different temperatures as prescribed in context of eq.(B27-B29). We show our results for $g_X = 10^{-8}$, $M_{Z'} = 10 \text{ MeV}$ for three different $U(1)_X$ charge combinations in Fig.10 assuming only tree level couplings (i.e. $\epsilon = 0$).

We consider $|X_1| = 1, |X_{2,3}| = 0$, $|X_1| = 0, |X_{2,3}| = 1$ and $|X_3| = -1, |X_{1,2}| = 0$ in Fig.10(a), Fig.10(b) and Fig.10(c) respectively. The red, blue and green lines indicate the temperature ratio T_{γ}/T_{ν_i} for ν_e, ν_{μ} and ν_{τ} respectively. Note that for $|X_1| = 1, |X_{2,3}| = 0$ only ν_e has BSM interactions which lead to enhancing T_{ν_e} , whereas $T_{\nu_{\mu/\tau}}$ reproduces the same value as predicted in SM scenario (where, $(T_{\gamma}/T_{\nu_i})_{\text{SM}} \sim 1.4$ [5]) as portrayed in Fig.10(a). It is interesting to note that this value of $N_{\text{eff}} = 3.09$ is less ($\sim 8\%$) than the one predicted for the same charge configuration in sec.3. This is due to the fact we overestimated the neutrino energy increment in presence of Z' while assuming all 3 ν_i share the same temperature.

For Fig.10(b) and Fig.10(c) also we notice the calculated values of N_{eff} is slightly less than what was predicted in sec.3. For $|X_1| = 0, |X_{2,3}| = 1$, Z' promptly decays to ν_{μ} and

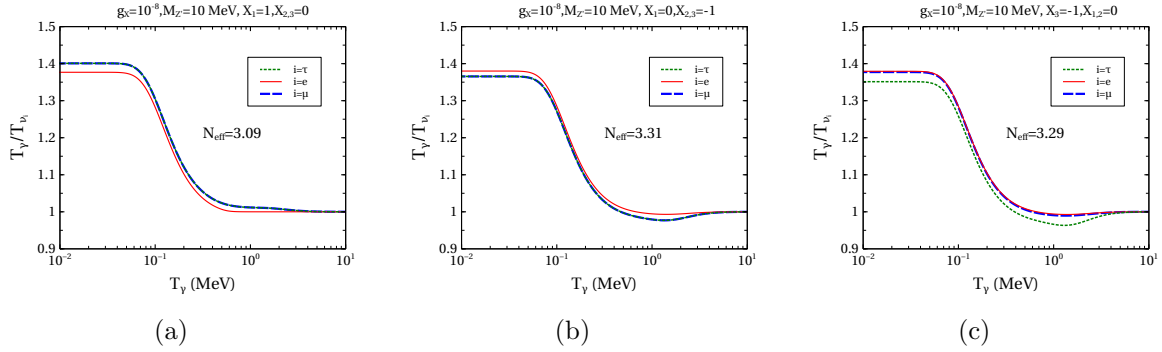


FIG. 10: Evolution of T_γ/T_ν with photon bath temperature T_γ assuming all 3 ν_i with different temperatures for different $U(1)_X$ charge combinations. We chose a benchmark parameter value $M_{Z'} = 10$ MeV and $g_X = 10^{-7}$ for all 3 plots. We consider 3 different charge combination (a) $X_1 = -1, X_{2,3} = 0$ (b) $X_2 = -1, X_{1,3} = 0$ and (a) $X_3 = -1, X_{1,2} = 0$. Here even if $X_1 = 0$ N_{eff} changes slightly depending on $X_{2,3}$ (in contrast to the case considered in the paper.)

ν_τ and not in electron. This causes a sudden dip (before $T_\gamma \approx 0.5$ MeV) in the respective temperature ratio curves shown by the blue and green line in Fig.10(b). For the same reason we notice similar dip in the temperature ratio curve (green line) for ν_τ in Fig.10(c). The value of N_{eff} is slightly higher for $|X_1| = 0, |X_{2,3}| = 1$ in Fig.10(b) compared to the one obtained for Fig.10(c) as the former one contains two type of ν_i having BSM interactions. Also it is worth pointing that the value of N_{eff} obtained for $|X_1| = 1, |X_{2,3}| = 0$ is less compared to the other two as here Z' decays to both ν_e and e (i.e. photon bath) whereas in the other two cases Z' decays only to ν_i bath.

-
- [1] S. Dodelson, *Modern Cosmology*. Academic Press, Amsterdam, 2003.
- [2] G. Mangano, G. Miele, S. Pastor, T. Pinto, O. Pisanti, and P. D. Serpico, “Relic neutrino decoupling including flavor oscillations,” *Nucl. Phys. B* **729** (2005) 221–234, [arXiv:hep-ph/0506164](#).
- [3] E. Grohs, G. M. Fuller, C. T. Kishimoto, M. W. Paris, and A. Vlasenko, “Neutrino energy transport in weak decoupling and big bang nucleosynthesis,” *Phys. Rev. D* **93** no. 8, (2016) 083522, [arXiv:1512.02205 \[astro-ph.CO\]](#).
- [4] **Planck** Collaboration, N. Aghanim *et al.*, “Planck 2018 results. VI. Cosmological parameters,” *Astron. Astrophys.* **641** (2020) A6, [arXiv:1807.06209 \[astro-ph.CO\]](#). [Erratum: *Astron. Astrophys.* 652, C4 (2021)].
- [5] M. Escudero, “Neutrino decoupling beyond the Standard Model: CMB constraints on the Dark Matter mass with a fast and precise N_{eff} evaluation,” *JCAP* **02** (2019) 007, [arXiv:1812.05605 \[hep-ph\]](#).
- [6] M. Escudero, D. Hooper, G. Krnjaic, and M. Pierre, “Cosmology with A Very Light $L_\mu - L_\tau$

- Gauge Boson,” *JHEP* **03** (2019) 071, [arXiv:1901.02010 \[hep-ph\]](#).
- [7] H. Esseili and G. D. Kribs, “Cosmological Implications of Gauged $U(1)_{B-L}$ on ΔN_{eff} in the CMB and BBN,” [arXiv:2308.07955 \[hep-ph\]](#).
- [8] S. Ganguly, S. Roy, and A. K. Saha, “Imprints of MeV scale hidden dark sector at Planck data,” *Phys. Lett. B* **834** (2022) 137463, [arXiv:2201.00854 \[hep-ph\]](#).
- [9] K. N. Abazajian and J. Heeck, “Observing Dirac neutrinos in the cosmic microwave background,” *Phys. Rev. D* **100** (2019) 075027, [arXiv:1908.03286 \[hep-ph\]](#).
- [10] V. Poulin, T. L. Smith, T. Karwal, and M. Kamionkowski, “Early Dark Energy Can Resolve The Hubble Tension,” *Phys. Rev. Lett.* **122** no. 22, (2019) 221301, [arXiv:1811.04083 \[astro-ph.CO\]](#).
- [11] D. K. Ghosh, S. Jeusun, and D. Nanda, “Long-lived inert Higgs boson in a fast expanding universe and its imprint on the cosmic microwave background,” *Phys. Rev. D* **106** no. 11, (2022) 115001, [arXiv:2206.04940 \[hep-ph\]](#).
- [12] D. K. Ghosh, P. Ghosh, and S. Jeusun, “CMB signature of non-thermal Dark Matter produced from self-interacting dark sector,” *JCAP* **07** (2023) 012, [arXiv:2301.13754 \[hep-ph\]](#).
- [13] V. Poulin, T. L. Smith, D. Grin, T. Karwal, and M. Kamionkowski, “Cosmological implications of ultralight axionlike fields,” *Phys. Rev. D* **98** no. 8, (2018) 083525, [arXiv:1806.10608 \[astro-ph.CO\]](#).
- [14] T. Bringmann, F. Kahlhoefer, K. Schmidt-Hoberg, and P. Walia, “Converting nonrelativistic dark matter to radiation,” *Phys. Rev. D* **98** no. 2, (2018) 023543, [arXiv:1803.03644 \[astro-ph.CO\]](#).
- [15] S.-P. Li and X.-J. Xu, “ N_{eff} constraints on light mediators coupled to neutrinos: the dilution-resistant effect,” *JHEP* **10** (2023) 012, [arXiv:2307.13967 \[hep-ph\]](#).
- [16] A. Biswas, D. K. Ghosh, and D. Nanda, “Concealing Dirac neutrinos from cosmic microwave background,” *JCAP* **10** (2022) 006, [arXiv:2206.13710 \[hep-ph\]](#).
- [17] M. Berbig, S. Jana, and A. Trautner, “The Hubble tension and a renormalizable model of gauged neutrino self-interactions,” *Phys. Rev. D* **102** no. 11, (2020) 115008, [arXiv:2004.13039 \[hep-ph\]](#).
- [18] M. Fabbrichesi, E. Gabrielli, and G. Lanfranchi, “The Dark Photon,” [arXiv:2005.01515 \[hep-ph\]](#).
- [19] **Borexino** Collaboration, T. Shutt, “Borexino: A status report,” *Nucl. Phys. B Proc. Suppl.* **110** (2002) 323–325.
- [20] A. Majumdar, D. K. Papoulias, and R. Srivastava, “Dark matter detectors as a novel probe for light new physics,” *Phys. Rev. D* **106** no. 1, (2022) 013001, [arXiv:2112.03309 \[hep-ph\]](#).
- [21] E. Ma and R. Srivastava, “Dirac or inverse seesaw neutrino masses from gauged $B-L$ symmetry,” *Mod. Phys. Lett. A* **30** no. 26, (2015) 1530020, [arXiv:1504.00111 \[hep-ph\]](#).

- [22] C. Bonilla, T. Modak, R. Srivastava, and J. W. F. Valle, “ $U(1)_{B_3-3L_\mu}$ gauge symmetry as a simple description of $b \rightarrow s$ anomalies,” *Phys. Rev. D* **98** no. 9, (2018) 095002, [arXiv:1705.00915 \[hep-ph\]](#).
- [23] B. Dutta, S. Ghosh, and J. Kumar, “Contributions to ΔN_{eff} from the dark photon of $U(1)_{T_{3R}}$,” *Phys. Rev. D* **102** no. 1, (2020) 015013, [arXiv:2002.01137 \[hep-ph\]](#).
- [24] **CMS** Collaboration, V. Khachatryan *et al.*, “Search for narrow resonances in dilepton mass spectra in proton-proton collisions at $\sqrt{s} = 13$ TeV and combination with 8 TeV data,” *Phys. Lett. B* **768** (2017) 57–80, [arXiv:1609.05391 \[hep-ex\]](#).
- [25] **ATLAS** Collaboration, G. Aad *et al.*, “Search for high-mass dilepton resonances using 139 fb^{-1} of pp collision data collected at $\sqrt{s} = 13$ TeV with the ATLAS detector,” *Phys. Lett. B* **796** (2019) 68–87, [arXiv:1903.06248 \[hep-ex\]](#).
- [26] A. Das, S. Oda, N. Okada, and D.-s. Takahashi, “Classically conformal $U(1)$ ’ extended standard model, electroweak vacuum stability, and LHC Run-2 bounds,” *Phys. Rev. D* **93** no. 11, (2016) 115038, [arXiv:1605.01157 \[hep-ph\]](#).
- [27] E. Accomando, L. Delle Rose, S. Moretti, E. Olaiya, and C. H. Shepherd-Themistocleous, “Extra Higgs boson and Z' as portals to signatures of heavy neutrinos at the LHC,” *JHEP* **02** (2018) 109, [arXiv:1708.03650 \[hep-ph\]](#).
- [28] P. Coloma, P. Coloma, M. C. Gonzalez-Garcia, M. C. Gonzalez-Garcia, M. Maltoni, M. Maltoni, J. a. P. Pinheiro, J. a. P. Pinheiro, S. Urrea, and S. Urrea, “Constraining new physics with Borexino Phase-II spectral data,” *JHEP* **07** (2022) 138, [arXiv:2204.03011 \[hep-ph\]](#). [Erratum: *JHEP* 11, 138 (2022)].
- [29] **COHERENT** Collaboration, D. Akimov *et al.*, “Measurement of the Coherent Elastic Neutrino-Nucleus Scattering Cross Section on CsI by COHERENT,” *Phys. Rev. Lett.* **129** no. 8, (2022) 081801, [arXiv:2110.07730 \[hep-ex\]](#).
- [30] E. Di Valentino, O. Mena, S. Pan, L. Visinelli, W. Yang, A. Melchiorri, D. F. Mota, A. G. Riess, and J. Silk, “In the realm of the Hubble tension—a review of solutions,” *Class. Quant. Grav.* **38** no. 15, (2021) 153001, [arXiv:2103.01183 \[astro-ph.CO\]](#).
- [31] A. G. Riess *et al.*, “Milky Way Cepheid Standards for Measuring Cosmic Distances and Application to Gaia DR2: Implications for the Hubble Constant,” *Astrophys. J.* **861** no. 2, (2018) 126, [arXiv:1804.10655 \[astro-ph.CO\]](#).
- [32] A. G. Riess *et al.*, “A 2.4 % Determination of the Local Value of the Hubble Constant,” *Astrophys. J.* **826** no. 1, (2016) 56, [arXiv:1604.01424 \[astro-ph.CO\]](#).
- [33] A. G. Riess *et al.*, “A Comprehensive Measurement of the Local Value of the Hubble Constant with 1 km/s/Mpc Uncertainty from the Hubble Space Telescope and the SH0ES Team,” *Astrophys. J. Lett.* **934** no. 1, (2022) L7, [arXiv:2112.04510 \[astro-ph.CO\]](#).
- [34] **Planck** Collaboration, P. A. R. Ade *et al.*, “Planck 2015 results. XIII. Cosmological parameters,” *Astron. Astrophys.* **594** (2016) A13, [arXiv:1502.01589 \[astro-ph.CO\]](#).
- [35] G. Efstathiou, “H0 Revisited,” *Mon. Not. Roy. Astron. Soc.* **440** no. 2, (2014) 1138–1152,

- arXiv:1311.3461 [astro-ph.CO].
- [36] W. L. Freedman, “Cosmology at a Crossroads,” *Nature Astron.* **1** (2017) 0121, arXiv:1706.02739 [astro-ph.CO].
- [37] J. L. Bernal, L. Verde, and A. G. Riess, “The trouble with H_0 ,” *JCAP* **10** (2016) 019, arXiv:1607.05617 [astro-ph.CO].
- [38] T. Araki, K. Asai, K. Honda, R. Kasuya, J. Sato, T. Shimomura, and M. J. S. Yang, “Resolving the Hubble tension in a $U(1)_{L_\mu-L_\tau}$ model with the Majoron,” *PTEP* **2021** no. 10, (2021) 103B05, arXiv:2103.07167 [hep-ph].
- [39] H. Hildebrandt *et al.*, “KiDS+VIKING-450: Cosmic shear tomography with optical and infrared data,” *Astron. Astrophys.* **633** (2020) A69, arXiv:1812.06076 [astro-ph.CO].
- [40] K. Akita, S. H. Im, and M. Masud, “Probing non-standard neutrino interactions with a light boson from next galactic and diffuse supernova neutrinos,” *JHEP* **12** (2022) 050, arXiv:2206.06852 [hep-ph].
- [41] S. Hannestad, “Oscillation effects on neutrino decoupling in the early universe,” *Phys. Rev. D* **65** (2002) 083006, arXiv:astro-ph/0111423.
- [42] R. N. Mohapatra and G. Senjanovic, “Neutrino Mass and Spontaneous Parity Nonconservation,” *Phys. Rev. Lett.* **44** (1980) 912.
- [43] J. Schechter and J. W. F. Valle, “Neutrino Masses in $SU(2) \times U(1)$ Theories,” *Phys. Rev. D* **22** (1980) 2227.
- [44] A. Fradette, M. Pospelov, J. Pradler, and A. Ritz, “Cosmological beam dump: constraints on dark scalars mixed with the Higgs boson,” *Phys. Rev. D* **99** no. 7, (2019) 075004, arXiv:1812.07585 [hep-ph].
- [45] C. D. Kreisch, F.-Y. Cyr-Racine, and O. Doré, “Neutrino puzzle: Anomalies, interactions, and cosmological tensions,” *Phys. Rev. D* **101** no. 12, (2020) 123505, arXiv:1902.00534 [astro-ph.CO].
- [46] M. Escudero Abenza, “Precision early universe thermodynamics made simple: N_{eff} and neutrino decoupling in the Standard Model and beyond,” *JCAP* **05** (2020) 048, arXiv:2001.04466 [hep-ph].
- [47] X. Luo, W. Rodejohann, and X.-J. Xu, “Dirac neutrinos and N_{eff} ,” *JCAP* **06** (2020) 058, arXiv:2005.01629 [hep-ph].
- [48] A. D. Dolgov and K. Kainulainen, “Fermi-Dirac corrections to the relic abundances,” *Nucl. Phys. B* **402** (1993) 349–359, arXiv:hep-ph/9211231.
- [49] M. Kawasaki, K. Kohri, and N. Sugiyama, “MeV scale reheating temperature and thermalization of neutrino background,” *Phys. Rev. D* **62** (2000) 023506, arXiv:astro-ph/0002127.
- [50] E. W. Kolb and M. S. Turner, *The Early Universe*, vol. 69. 1990.
- [51] E. K. Akhmedov, “Neutrino physics,” in *ICTP Summer School in Particle Physics*, pp. 103–164. 6, 1999. arXiv:hep-ph/0001264.

- [52] A. D. Dolgov, “Neutrinos in cosmology,” *Phys. Rept.* **370** (2002) 333–535, [arXiv:hep-ph/0202122](#).
- [53] A. D. Dolgov, S. H. Hansen, S. Pastor, S. T. Petcov, G. G. Raffelt, and D. V. Semikoz, “Cosmological bounds on neutrino degeneracy improved by flavor oscillations,” *Nucl. Phys. B* **632** (2002) 363–382, [arXiv:hep-ph/0201287](#).
- [54] D. W. P. d. Amaral, D. G. Cerdeno, P. Foldenauer, and E. Reid, “Solar neutrino probes of the muon anomalous magnetic moment in the gauged $U(1)_{L_\mu-L_\tau}$,” *JHEP* **12** (2020) 155, [arXiv:2006.11225 \[hep-ph\]](#).
- [55] H. Banerjee, B. Dutta, and S. Roy, “Probing $L_\mu-L_\tau$ models with CE ν NS: A new look at the combined COHERENT CsI and Ar data,” *Phys. Rev. D* **104** no. 1, (2021) 015015, [arXiv:2103.10196 \[hep-ph\]](#).
- [56] D. K. Ghosh, P. Ghosh, S. Jeesun, and R. Srivastava, “Probing $U(1)_X$ models from cosmology and ground based experiments,” [arXiv:2401.xxxx \[hep-ph\]](#).
- [57] XENON Collaboration, E. Aprile *et al.*, “The XENON1T Dark Matter Experiment,” *Eur. Phys. J. C* **77** no. 12, (2017) 881, [arXiv:1708.07051 \[astro-ph.IM\]](#).
- [58] K. Chakraborty, A. Das, S. Goswami, and S. Roy, “Constraining general $U(1)$ interactions from neutrino-electron scattering measurements at DUNE near detector,” *JHEP* **04** (2022) 008, [arXiv:2111.08767 \[hep-ph\]](#).
- [59] M. Cadeddu, N. Cargioli, F. Dordei, C. Giunti, Y. F. Li, E. Picciau, and Y. Y. Zhang, “Constraints on light vector mediators through coherent elastic neutrino nucleus scattering data from COHERENT,” *JHEP* **01** (2021) 116, [arXiv:2008.05022 \[hep-ph\]](#).
- [60] E. W. Kolb and M. S. Turner, “Supernova SN 1987a and the Secret Interactions of Neutrinos,” *Phys. Rev. D* **36** (1987) 2895.
- [61] P.-W. Chang, I. Esteban, J. F. Beacom, T. A. Thompson, and C. M. Hirata, “Toward Powerful Probes of Neutrino Self-Interactions in Supernovae,” *Phys. Rev. Lett.* **131** no. 7, (2023) 071002, [arXiv:2206.12426 \[hep-ph\]](#).
- [62] H. T. Janka, “Neutrino Emission from Supernovae,” [arXiv:1702.08713 \[astro-ph.HE\]](#).
- [63] D. Croon, G. Elor, R. K. Leane, and S. D. McDermott, “Supernova Muons: New Constraints on Z' Bosons, Axions and ALPs,” *JHEP* **01** (2021) 107, [arXiv:2006.13942 \[hep-ph\]](#).
- [64] W. Altmannshofer, S. Gori, M. Pospelov, and I. Yavin, “Neutrino Trident Production: A Powerful Probe of New Physics with Neutrino Beams,” *Phys. Rev. Lett.* **113** (2014) 091801, [arXiv:1406.2332 \[hep-ph\]](#).
- [65] M. D. Schwartz, *Quantum Field Theory and the Standard Model*. Cambridge University Press, 3, 2014.
- [66] Particle Data Group Collaboration, R. L. Workman *et al.*, “Review of Particle Physics,” *PTEP* **2022** (2022) 083C01.
- [67] A. S. de Jesus, N. Pinto-Neto, F. S. Queiroz, J. Silk, and D. R. da Silva, “The hubble rate trouble: an effective field theory of dark matter,” *Eur. Phys. J. C* **83** no. 3, (2023) 203,

- [arXiv:2212.13272](#) [hep-ph].
- [68] **CMB-S4** Collaboration, K. Abazajian *et al.*, “Snowmass 2021 CMB-S4 White Paper,” [arXiv:2203.08024](#) [astro-ph.CO].
- [69] A. R. Zhitnitsky, “Confinement Deconfinement Phase Transition in Hot and Dense QCD at Large $N(c)$,” *Nucl. Phys. A* **813** (2008) 279–292, [arXiv:0808.1447](#) [hep-ph].